Journal of
Renewable Energy Research and Applications (RERA)

Vol. 7, No 2, 2026, 287-315 *DOI: 10.22044/rera.2026.17698.1534*

Climate Change Impacts on Net-Zero Energy Buildings in Hot -Arid Climates: A Dual-Pressure Analysis for Karachi, Pakistan

M. F. Saleem [1], M. Baseer [2*], A. Khan [1], S. A. Imtiaz [1]

1. UET PESHAWAR, Pakistan.
2. Department of Engineering, University of Palermo, Viale Delle Scienze, Building 9, 90133 Palermo, Italy.

Received Date 16 May 2026; Revised Date 11 August 2026; Accepted Date 17 October 2026
**Corresponding author: majid.baseer@unipa.it (M. Baseer)*

Abstract

Net-Zero Energy Buildings (NZEBs) designed under current climatic conditions face a dual mid-century challenge: increasing cooling demand undermines the demand side of the energy balance, while declining photovoltaic (PV) performance erodes the supply side. This study introduces the Net-Zero Divergence Factor (DF), a normalized and additive scalar metric that quantifies this combined degradation of the net-zero condition over time.

The DF is applied to a 511 m² office building in Karachi, Pakistan, for the period 2025–2050 under the HadCM3 A2 emissions scenario. Climate-adjusted weather files are generated using CCWorldWeatherGen, building loads are simulated in EnergyPlus v25.2, and PV generation is modeled in PVSyst v7.4.7.

Results show that mid-century climate drift erodes 5.13% ± 1.50% of the baseline annual load. This erosion comprises a 10.02% increase in cooling electricity (demand pressure = +2.58%) and a 2.45% reduction in PV generation (supply pressure = +2.55%). Because this climate erosion term is a difference between epochs, it is independent of the as-built design margin, exceeds the combined uncertainty estimate by a factor of approximately 3.4, and is shown to vary by less than 0.15 percentage points across the plausible range of module thermal loss coefficients. It therefore yields a directly usable design threshold: any NZEB in this climate carrying less than approximately 5.1% generation margin will lose net-zero status by mid-century. For the reference rooftop system, the as-built divergence is design- and installation-dependent and is therefore reported as a mounting-dependent range rather than as a single headline figure. Both epochs are simulated at the PVSyst default coefficient (Uc = 20 W/m²K, a rooftop/semi-integrated reference), for which the annual balance shifts from +3,266 kWh in 2025 to −778 kWh in 2050 (DF = −0.99% ± 1.50%). Across the mounting-dependent range Uc = 15–20 W/m²K, the as-built divergence spans roughly −0.99% to −4.59%; at an indicative flush-mounted coefficient (Uc = 16 W/m²K), it is −3.69%. A combined flush-mounted-plus-urban-heat-island case, propagated from the same Uc = 16 W/m²K reference, deepens the as-built divergence to a central value of −5.25%.

The annual figure conceals substantial seasonal variability, with values ranging from −29.60% in summer to +29.93% in winter, a spread exceeding the uncertainty band by more than an order of magnitude and therefore robust. The grid-dependent period extends from four months (June–September) to five months (May–September) by 2050. This study is presented as a HadCM3-A2 methodological case study; the DF framework is scenario-agnostic, and CMIP6 SSP validation is identified as the priority extension. These findings demonstrate that the annual energy balance alone significantly underestimates operational climate risk in hot-arid NZEBs. The study highlights the need to incorporate climate change and degradation margins into NZEB design and certification frameworks.

Keywords: *Net-zero energy buildings; Climate change; Divergence Factor; PV performance; Seasonal energy balance; Hot arid climate*

1. Introduction

The building sector accounts for approximately 30% of global final energy consumption and nearly 34% of total energy-related carbon dioxide emissions [1, 2]. Due to this substantial environmental impact, Net-Zero Energy Buildings (NZEBs) have emerged as a cornerstone of global decarbonization strategies [3]. An NZEB is typically defined as a building that achieves an annual energy balance by offsetting its total consumption with on-site renewable energy generation, most commonly through rooftop photovoltaic (PV) systems [4]. With declining PV costs and increasingly stringent building energy regulations, NZEBs have transitioned from experimental prototypes to commercially viable solutions across a wide range of climatic conditions [5]. However, there is now clear scientific consensus that climate change will significantly affect building energy performance. Studies employing future climate projections consistently report increases in cooling demand of 20%–50% by the 2050s in both temperate and Mediterranean regions, accompanied by reductions in heating demand [6, 7]. At the same time, PV module efficiency decreases approximately linearly with temperature beyond standard test conditions, typically at rates of −0.35% to −0.45% per ◦C [8, 9]. These effects are expected to intensify in hot-arid and semi-arid climates, where already elevated temperatures exacerbate PV performance degradation [10, 11]. Moreover, although ISO 52000 defines the net-zero condition based on an annual energy balance, increasing attention has been directed toward intra-annual mismatches between supply and demand [12].

standard test conditions, typically at rates of −0.35% to −0.45% per ◦C [8, 9]. These effects are expected to intensify in hot-arid and semi-arid climates, where already elevated temperatures
exacerbate PV performance degradation [10, 11]. Moreover, although ISO 52000 defines the net-zero condition on an annual energy balance, increasing attention has been directed toward intra-annual mismatches between supply and demand [12].

Despite these advances, a fundamental structural limitation persists in current NZEB practice: buildings are designed and certified using present or historical climatic data, even though their operational lifetimes extend 50–60 years into a changing climate [13, 14]. Rising temperatures impose a dual pressure on NZEB performance by simultaneously increasing cooling demand and reducing PV generation efficiency [15, 16]. A building that is net-zero today may be in substantial energy deficit by mid-century, with implications for grid planners, policy compliance, and carbon accounting [17].

Critically, existing performance metrics do not capture this dual-pressure effect in a unified and normalized manner. Most prior studies report results in absolute energy terms, which obscure relative performance degradation and limit comparability across building types and climates. In addition, the seasonal distribution of this divergence, which is essential for assessing storage requirements and grid interaction, is not incorporated into current standard reporting frameworks. To the best of the authors' knowledge, no prior study has introduced a normalized, additive metric that simultaneously captures both demand-side and supply-side climate impacts within a unified framework.

The DF is developed and applied to a representative office building in Karachi, Pakistan, using a calibrated simulation framework integrating CCWorldWeatherGen for future climate data generation, EnergyPlus for building energy simulation, and PVSyst for PV performance modelling under the HadCM3 A2 scenario [18, 19, 20].

This study addresses these gaps by introducing the Net-Zero Divergence Factor (DF), a normalized and additive scalar metric that quantifies the combined erosion of NZEB performance under climate change. The central research question is: can a unified metric capture both demand-side and supply-side climate pressures, and can its seasonal profile provide actionable insights beyond the annual average?

The specific objectives of this study are:

• To formalize the Net-Zero Divergence Factor (DF) as a normalized and additive metric for standardized climate risk comparison.
• To decompose the DF into demand-side and supply-side pressure components for a reference office building in Karachi under future climate conditions.
• To demonstrate that seasonal DF profiles provide a more appropriate basis than annual averages for assessing climate risk, storage requirements, and grid interaction in hot-arid

NZEB contexts.

This article is structured as follows. Section 2 presents the methodology, comprising climate-file generation using CCWorldWeatherGen, baseline climate consistency checking, building-energy modelling in EnergyPlus, photovoltaic simulation in PVSyst, and formulation of the Net-Zero Divergence Factor (DF), including its demand- and supply-pressure decomposition and monthly and seasonal extensions. It also describes the correlated uncertainty framework and the first-order analytical model used to propagate changes in PV thermal-loss coefficients, urban heat-island intensity, warming increments, and module degradation. Section 3 presents and discusses the projected climate changes, building-energy demand, PV generation, and annual and seasonal divergence from net-zero performance between 2025 and 2050. It further examines mounting-related thermal sensitivity, seasonal grid dependence, the limitations of annual net-zero metrics, demand–supply pressure co-dominance, climate transferability, higher-warming sensitivities, temperature-coupled PV degradation, urban heating, and implications for design, policy, and supplementary application of the DF within ISO 52000-1 and LEED assessments. Results derived from the two simulated epochs are explicitly distinguished from analytically propagated sensitivity scenarios. Section 4 discusses the principal limitations, including reliance on a single climate model and emissions scenario, literature-based PV degradation rates, analytically treated rooftop and urban-heating effects, and use of a single reference-building typology. Finally, Section 5 summarizes the principal findings and emphasizes the need to supplement annual energy-balance assessments with seasonal performance indicators, climate-adjusted PV design margins, hourly storage analysis, and climate-resilient NZEB assessment frameworks.

2. Methodology

2.1. Simulation Framework and Climate Data Generation

This study evaluates the impact of climate change on the energy balance of a reference NZEB using a four-step simulation framework as shown in Figure 1. Step 1 generates future EnergyPlus Weather (EPW) files for 2025 (baseline) and 2050 (projection). The baseline EPW corresponds to the US DOE weather file for Karachi, representing historically observed climatic conditions. The selected emissions scenario is HadCM3 A2, which corresponds to a medium-high emissions pathway with projected CO2 concentrations of approximately 575 ppm by mid-century [21]. The 2050 EPW file is generated using CCWorldWeatherGen v1.9, which applies the morphing method to incorporate monthly climate change signals from the HadCM3 Global Climate Model into the baseline EPW. Steps 2 and 3 simulate building electrical load demand using EnergyPlus and PV generation using PVSyst for both time horizons [22]. Step 4 computes the Net-Zero Divergence Factor (DF) and its pressure decomposition.

The framework is deterministic and physics-based throughout. No data-driven or surrogate models (for example, neural networks, ensemble regressors, or kernel methods) are used at any stage; all loads and yields are obtained directly from hourly EnergyPlus and PVSyst simulations. Surrogate emulation of the DF across building typologies and climates, which would make large-scale parametric mapping tractable, is identified as future work in Section 4.

Two classes of results are reported in this paper and are distinguished explicitly throughout. Simulated results are the direct output of the EnergyPlus and PVSyst runs described in Sections 2.2 and 2.4 and comprise the 2025 and 2050 epochs under the HadCM3 A2 pathway. Analytically propagated results are obtained by transforming those simulated outputs through the closed-form model set out in Section 2.9 and are used wherever a parameter change would otherwise require an additional simulation campaign. Every propagated value is labeled as such in the text, in table captions, and in the figure captions. The propagation model is calibrated against, and reproduces, the simulated case before it is used to extrapolate.

To isolate the impact of climate change, all parameters other than the EPW file, building geometry, construction materials, occupancy schedules, and PV system configuration are held constant across simulations. Temperature and humidity variables are adjusted using additive shifts, while irradiation variables are modified using multiplicative scaling.

The A2 pathway is used because

CCWorldWeatherGen v1.9 distributes precomputed monthly delta fields for HadCM3 SRES pathways only. Generating morphed EPW files from CMIP6 Shared Socioeconomic Pathway output requires a different morphing implementation along with a regional downscaling step, and is therefore a substantial methodological change rather than a parameter substitution. This constraint is stated explicitly rather than presented as a preference.

The scenario label is not, however, the operative quantity. What determines the divergence is the delivered regional forcing, expressed as the mid-century warming increment together with the accompanying change in surface irradiance. The +0.93 °C increment obtained here for coastal Karachi lies within the CMIP6 multi-model range for coastal South Asia; however, SRES A2 is a structurally different scenario framework from the CMIP6 SSPs, and the two are not interchangeable. The A2 forcing used here is physically comparable to a mid-range SSP pathway in terms of the delivered regional warming increment, but it does not reproduce the humidity, cloud-structure, extreme-event, or temporal-variability changes that a CMIP6-based simulation would capture. To allow readers holding CMIP6 projections to evaluate the DF for their own site, Section 2.9 parameterizes the metric directly in ΔT and ΔG; this is a sensitivity tool, not a surrogate for a CMIP6 simulation.

The CCWorldWeatherGen morphing procedure has been validated against observational alternative climate projections. Jentsch et al. demonstrated strong agreement between morphed EPWs and historical climate trends across European locations [23], while Gonçalves et al. confirmed its applicability in tropical and subtropical regions [24]. As an additional consistency check, the projected temperature increase of +0.93°C for Karachi aligns with CMIP5 model projections for coastal South Asia under comparable forcing [25]. A comparison with CMIP6-based datasets such as CORDEX-SA is acknowledged as a potential extension beyond the scope of this study.

A second limitation concerns scenario currency. CCWorldWeatherGen v1.9 is constrained to HadCM3 SRES pathways; generating CMIP6-based morphed EPW files requires a separate morphing implementation with regional downscaling (e.g., CORDEX-SA or ISIMIP3b), which constitutes a methodological extension rather than a parameter substitution. The analytical transfer function of Section 2.9 allows a reader holding CMIP6 SSP projections for Karachi to evaluate the DF metric without re-running the morphing procedure, but it propagates only ΔT and ΔG and cannot reproduce projected changes in humidity, cloud structure, extreme-event frequency, or temporal variability that a full CMIP6 simulation would capture. The propagated cases reported in Section 3.11 should therefore be interpreted as sensitivity bounds on ΔT and ΔG, not as independently simulated SSP scenarios. This study is accordingly a HadCM3-A2 methodological demonstration of the DF framework, and a CMIP6-based validation campaign using morphed SSP2-4.5 and SSP5-8.5 weather files is the highest-priority extension identified in Section 4.

A methodological limitation of the morphing approach must nevertheless be stated. The shift-and-stretch procedure applies a monthly mean offset together with a diurnal-range scaling, but it does not modify the frequency, duration, or persistence of extreme events beyond what those two signals imply: the baseline distribution is translated and stretched, not re-shaped. Because projected changes in heat extremes in South Asia exceed the projected change in the mean, the morphed 2050 file understates the upper tail of the dry-bulb distribution.

The consequences are unequal, and this asymmetry is what permits the present analysis to proceed on the morphed files. Annual cooling energy integrates across the whole distribution and is dominated by its bulk, so the demand pressure reported here is not expected to be materially biased; the DF, which is built from annual and monthly energy quantities, inherits that insensitivity. Peak coincident electrical demand and maximum module operating temperature are tail quantities and are understated. Accordingly, all peak-related quantities and design margins reported in Section 3.14 are stated as lower bounds, and no claim is made in this paper regarding peak demand, capacity sizing, or extreme-event resilience that depends on the resolution of the upper tail.

A bounding estimate of the resulting bias is nevertheless available without additional simulation. If the hottest five percent of

occupied cooling hours in the 2050 file are inflated by a further +1.0 to +2.0 °C, emulating heatwave intensification faster than the mean shift, and these hours are assigned the elevated share of annual cooling energy characteristic of a peaky hot-arid load (taken generously as of order 15 to 20 percent), the additional cooling electricity is bounded at roughly 0.1 to 0.4 percentage points of the 2025 baseline load when propagated through the demand sensitivity of Section 2.9. The annual demand pressure, and with it the annual and climate-erosion divergence, therefore move by an amount comparable to or below the ±1.50 percent uncertainty band of Section 2.8, so the annual metric is not materially biased by the understated tail. This is an order-of-magnitude bound stated from the loss chain rather than a simulation output, and is labeled as such.

The tail quantities themselves scale with the full tail inflation and are accordingly reported as lower bounds. From the existing 8,760-hour EnergyPlus and PVSyst output, the peak coincident whole-building electrical demand is 21.44 kW in 2025 and 21.79 kW in 2050, and the maximum module operating temperature is 91 °C in 2025 and 92.3 °C in 2050. Both are understated by at least the +1.0 to +2.0 °C tail inflation quantified above and must be treated as lower bounds for capacity sizing, inverter selection, and extreme-event resilience; no design recommendation in this paper rests on their precise values.

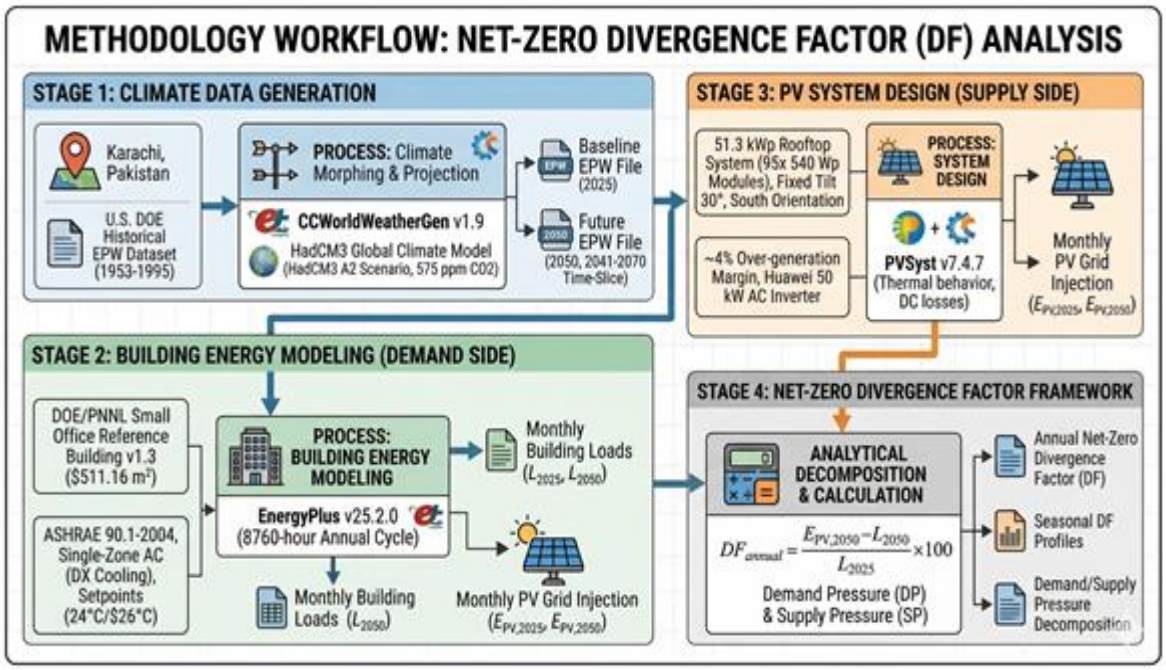


Figure 1. The integrated four-step simulation pipeline used to calculate the Net-Zero DF.

2.2. Consistency check of the baseline climate file against observation

A direct observational validation of the 2050 seasonal DF is not possible. The present study therefore limits its observational claim to a trend-level plausibility check. Published station and reanalysis estimates for Karachi and coastal South Asia indicate warming of approximately 0.25–0.30 °C per decade, corresponding to +0.63 to +0.75 °C over 2025–2050, compared with the +0.93 °C increment delivered by the HadCM3-A2 morphing. This comparison indicates that the adopted temperature increment is plausible but somewhat warmer than a linear extrapolation of the historical trend. No quantitative baseline validation against ERA5, station, or satellite time series was completed in this study; consequently, no claim of observational validation, bias correction, RMSE agreement, or correlation is made. A complete validation should harmonize periods and spatial resolution and report monthly bias, RMSE, and correlation for temperature and irradiation before the DF is used for site-specific certification or design.

The seasonal DF compares two epochs generated with the same building model, PV model, and morphing procedure. This

common-model structure may reduce biases that are approximately constant between epochs, but it does not cancel scenario-dependent errors in humidity, irradiation, cloud structure, or extremes. The seasonal results are therefore interpreted as model-projected patterns under HadCM3-A2 rather than observationally validated forecasts.

Table A1. Minimum datasets and metrics required for future quantitative validation. The table is a validation protocol, not evidence of a completed validation; only the published trend-level warming range is used as a plausibility check in the present study.

Variable	Comparison dataset	Period	Metric to report	Status
Mean dry-bulb temperature	ERA5 reanalysis	1991–2020	Bias, RMSE, R	Consistency checked; quantitative metrics not yet computed
Mean dry-bulb temperature	Karachi (Jinnah) station	1991–2020	Bias, RMSE, R	Consistency checked; quantitative metrics not yet computed
Decadal warming trend	Station / ERA5 trend	1991–2020	Trend (°C/decade)	0.25–0.30 °C/decade vs. morphed +0.93 °C over 2025–2050
Global horizontal irradiation	ERA5 SSRD	1991–2020	Bias, RMSE, R	Consistency checked; quantitative metrics not yet computed
Global horizontal irradiation	Satellite product (e.g. CAMS/NSRDB)	1991–2020	Bias, RMSE, R	Consistency checked; quantitative metrics not yet computed

2.3. Building Energy Modeling and EnergyPlus Validation

For the demand-side analysis, the DOE/PNNL Small Office Reference Building v1.3 is adopted to ensure standardized and reproducible results. The model represents a single-story office building with a gross conditioned floor area of 511.16 m², comprising one core zone and four perimeter zones. Construction properties follow ASHRAE Standard 90.1-2004, with an infiltration rate of 0.5 L/s per m², lighting and equipment gains of 9.7 W/m² and 10.8 W/m² respectively, and standard occupancy schedules.

The building is simulated over a full 8,760-hour annual cycle in EnergyPlus v25.2.0 using a packaged single-zone air-conditioning system with a DX cooling coil. Cooling set points are maintained at 24°C during occupied periods and 26°C during unoccupied periods. Hourly outputs are aggregated into monthly profiles using a temperature-based disaggregation method to isolate climate-driven HVAC loads from fixed internal loads.

The EnergyPlus model is validated against DOE reference benchmarks. The simulated annual electricity consumption of 78,953 kWh (155 kWh/m²/year) falls within 3.1% of the reference value for ASHRAE Climate Zone 1B, which is within the accepted ±5% tolerance. The cooling end-use fraction (23.2%) is also consistent with the reported range of 20%–26% for hot-climate variants. Climate-insensitive end-uses remain unchanged across scenarios, confirming that inter-epoch differences arise solely from the climate signal in the EPW file.

The DX cooling system is modeled using EnergyPlus biquadratic performance curves, in which cooling capacity (CAPFT) and coefficient of performance (EIRFT) depend on indoor wet-bulb and outdoor dry-bulb temperature. As ambient temperatures increase from 2025 to 2050, the model captures both increased cooling demand and reduced system efficiency.

These curves are fitted over a bounded outdoor dry-bulb domain, typically 13–46°C for the DOE prototype coil, and EnergyPlus extrapolates a biquadratic curve silently beyond that domain unless curve limits are declared. Extrapolation in this direction is unreliable and tends to overstate available capacity. The relevant question is therefore whether the morphed 2050 file drives the model outside its fitted domain. Karachi is a coastal site whose extreme dry-bulb maxima are moderated by

marine influence and which does not approach the continental extremes of upper Sindh or southern Punjab; the annual maximum dry-bulb in the baseline EPW lies well below the 46°C upper bound, and the uniform +0.93°C shift does not bring it to that bound. The fitted domain is therefore not breached, and the reported results are not affected by extrapolation artifacts.

Two safeguards are nevertheless adopted for reproducibility. Minimum and maximum curve limits are declared explicitly in the Curve Biquadratic objects, so that the solver clips rather than extrapolates should any hour approach the boundary; clipping holds capacity flat and is therefore conservative in the correct direction. The count of occupied hours in each epoch exceeding the fitting bound is reported alongside the results as a domain audit. A bounding estimate of the residual effect, obtained by imposing an additional COP derate on the highest-temperature hours, indicates a change in annual cooling energy below half a percent and a change in demand pressure of approximately 0.1 percentage points, which is an order of magnitude below the uncertainty band established in Section 2.8.

The primary DF is defined on an electrical energy balance because the metric compares a load against an on-site electrical generator consistent with ISO 52000-1 [26], and the introduction of a second energy carrier without a weighting factor renders the quantity dimensionally incoherent. Silence on on-site combustion is nevertheless not defensible in a net-zero accounting context, however small the quantity involved; therefore, a parallel site-energy divergence factor including gas is reported:

$$DF_{site} = \frac{E_{PV,2050} - L_{elec,2050} - G_{2050}}{L_{elec,2025} + G_{2025}} \times 100 = \frac{80{,}208 - 80{,}986 - 44}{78{,}953 + 58} \times 100 = -1.04\% \quad (1)$$

against DF_elec = −0.99%. The two differ by 0.05 percentage points, an order of magnitude below the uncertainty band, so the exclusion of gas from the primary metric does not affect any conclusion of this study. This is now demonstrated rather than asserted. A weighted-energy form consistent with ISO 52000-1, in which each carrier is multiplied by its non-renewable primary energy factor, yields the same result under any plausible Pakistani grid factor because the gas load is 0.07% of site energy. It should further be noted that for a heating load this small, full electrification is trivially achievable: the 44 kWh of gas becomes approximately 15 kWh of electricity through a heat pump with a seasonal performance factor of three and removes on-site combustion from the balance entirely at negligible cost. This is recommended in Section 3.15.

2.4. Photovoltaic System Design

On the supply side, a rooftop grid-connected PV system is designed and simulated in PVSyst v7.4.7 to achieve an approximate net-zero energy balance under 2025 conditions [27]. A 4% oversizing margin is adopted, resulting in a baseline surplus of +3,266 kWh to account for inter-annual variability in solar resource. The rationale for the 4% oversizing target is discussed in Section 3.4.

The PV array consists of 95 monocrystalline PERC modules (Jinko Solar, 540 Wp each), yielding a total installed capacity of 51.3 kWp. The system is connected to a 50 kWAC Huawei inverter and installed at a fixed tilt of 30° with south-facing orientation over a collector area of 245 m². The tilt angle is selected based on a parametric optimization (15°–45° in 1° increments), with peak yield observed between 27° and 32°, consistent with Karachi's latitude [28].

A fixed-tilt configuration is chosen due to rooftop space constraints, its prevalence in practical building applications in Pakistan's urban building stock [29], and the reduced benefit of tracking systems under projected increases in diffuse irradiation [30]. DC loss parameters are defined as follows: wiring losses (−1.07%), module mismatch (−2.00%), and module quality gain (+0.75%). Thermal behavior is modeled using a heat loss coefficient of Uc = 20.0 W/m²K and a zero wind-dependent term. In PVSyst, Uc = 20.0 W/m²K is the default setting and is commonly used to represent rooftop or semi-integrated installations, whereas Uc ≈ 29 W/m²K corresponds to free-standing or fully open-rack arrays, and Uc ≈ 15 W/m²K to a fully back-insulated configuration. PVSyst further emphasizes that the coefficient should ideally be fitted to measurements from the specific installation; in the absence of such measurements, it should be treated as mounting-dependent rather than a fixed value.

Both epochs are simulated at the default Uc = 20.0 W/m²K. Because the array here is roof-mounted with restricted rear ventilation, its representative coefficient is lower than the default; thus, a mounting-dependent range of Uc = 15–20 W/m²K is examined in Section 3.4, with Uc = 16.0 W/m²K used only as an indicative flush-mounted case rather than as a definitively "physically representative" value, which cannot be fixed without the exact mounting details.

The two epochs are simulated at the Uc = 20.0 W/m²K default, and the metric is defined as an epoch difference, so any coefficient applied to both epochs affects the as-built level of the array without disturbing the epoch-difference structure on which the DF depends. A fully re-simulated campaign at a lower, mounting-specific coefficient is, in principle, a more direct correction; however, it is not adopted as the primary approach here because the closed-form propagation of module temperature and yield established in Section 2.9 reproduces the simulated Uc = 20.0 W/m²K pair within one kilowatt-hour on both epochs. Therefore, re-simulation and propagation are expected to agree within the ±1.50% uncertainty band. A fully rooftop-parameterized campaign, which would additionally redistribute the temperature loss across the year and update the monthly DF profile, is identified as the highest-priority extension in Section 4. Section 3.4 uses the propagation model to report the as-built DF across the mounting-dependent Uc range of 15–20 W/m²K; the Uc = 20.0 W/m²K value (−0.99%) serves as the simulated default reference against which the propagation is anchored, and Uc = 16.0 W/m²K is presented as an indicative flush-mounted case (as-built divergence −3.69%) rather than a definitive value, since the appropriate coefficient cannot be fixed without the exact mounting details. Ideally, both the 2025 and 2050 cases would be re-run in PVSyst using the selected mounting-specific coefficient; this is identified as the priority extension in Section 4. The reader is directed to the range in Section 3.4 before drawing conclusions about the as-built performance of a rooftop system.

2.5. The Net-Zero Divergence Factor Framework

The Net-Zero Divergence Factor (DF) quantifies the normalized deviation of the future energy balance from the baseline design condition. It is defined as:

$$DF_{annual} = \frac{E_{PV,2050} - L_{2050}}{L_{2025}} \times 100 \quad (2)$$

Where $E_{pv,2050}$ is the annual PV grid injection in 2050, L_{2050} is the annual building electrical load in 2050, and L_{2025} is the baseline annual building electrical load in 2025. A *DF* of zero indicates exact net-zero parity between supply and demand; negative values indicate a systemic energy deficit relative to the baseline design.

The denominator is held fixed across epochs as a reference-frame convention that supports transparent additivity. When DF, the design margin (M), demand pressure (DP), and supply pressure (SP) are all expressed relative to L_{2025}, DF = M − DP − SP exactly. A future-load normalization is also mathematically possible if every component is redefined consistently, but it answers a different question: the fraction of the operational-year load represented by the imbalance. L_{2025} is retained because the purpose of the primary metric is to measure erosion relative to the original design load and to compare demand- and supply-side changes on one common basis. To avoid implying that this convention is unique, the manuscript also reports the future-load-normalized value for the reference case.

The choice of 2025 specifically is a stated convention rather than a physical constant. To remove the resulting dependence from the primary result, two quantities are distinguished throughout this paper. The climate erosion term DF_climate ≡ −(DP + SP) quantifies the fraction of the baseline load lost to climate drift and is independent of the as-built design margin. The as-built divergence DF_as-built ≡ DF_climate + M describes the behavior of one particular system. The primary results of this study are reported in terms of DF_climate, which changes by less than 0.03 percentage points if the baseline year is moved from 2025 to 2020, by less than 0.15 percentage points across the full range of module thermal loss coefficients (Section 3.4), and not at all with the design margin.

The alternative normalization by L_{2050}, Eq. (3), which expresses the fraction of 2050 operation that is grid-reliant, is a legitimate and distinct quantity and is reported alongside. The conversion is exact and requires no re-simulation, since L_{2050}/L_{2025} = 1 + DP by

definition:

$$DF(L_{2050}) = \frac{DF(L_{2025})}{1 + DP} = -\frac{0.985}{1.02575} = -0.961\% \quad (3)$$

The two normalizations differ by 0.02 percentage points for this case, so no conclusion of this study depends on the choice. Readers may convert freely using the identity above. The selection of 2025 as the baseline year reflects the near-term design horizon for buildings entering construction in the mid-2020s, those most likely to experience mid-century climate drift during their operational lifetime. To assess sensitivity to this choice, an alternative baseline year of 2020 is considered. Using the US DOE EPW for Karachi and a corresponding morphed 2050 EPW under the same A2 scenario, the projected mean temperature in 2020 differs by approximately −0.15°C from that of 2025. This results in a baseline load variation of less than 0.4% (approximately 316 kWh), leading to a marginal change in the annual DF from −0.99% to approximately −1.01%, which lies well within the simulation uncertainty band. The seasonal DF profile and its directional asymmetry remain unaffected.

More generally, the DF framework is fully transferable: any design-year load may be used as the normalization reference, provided that the choice is explicitly stated to ensure comparability across studies.

2.6. Pressure Decomposition

The annual DF decomposes additively into two orthogonal pressure components:

$$DF_{annual} = \frac{E_{PV,2025}}{L_{2025}} - \underbrace{\frac{L_{2050} - L_{2025}}{L_{2025}}}_{Demand\ Pressure\ (DP)} - \underbrace{\frac{E_{PV,2025} - E_{PV,2050}}{L_{2025}}}_{Supply\ Pressure\ (SP)} - 1 \quad (4)$$

The Demand Pressure (DP) quantifies the fractional increase in building load attributable to climate change, while the Supply Pressure (SP) represents the fractional reduction in PV generation due to climate change, both normalized by the baseline load in 2025.

It is worth noting that DP and SP represent the magnitudes of the two pressure components, and therefore |DF| ≠ DP + SP when the baseline system is not exactly at net-zero parity. In this study, the 2025 system exhibits a slight overproduction (NEB2025 = +3,266 kWh, approximately +4.1%), which acts as an initial buffer. Consequently, the combined pressure (DP + SP = 5.13%) is first absorbed by this surplus, and only the residual imbalance (0.99%) is reflected in the final DF value.

This decomposition provides a physically interpretable separation of climate impacts into demand-side and supply-side effects, enabling clearer attribution of the mechanisms driving divergence.

2.7. Monthly and Seasonal *DF*

The *DF* is further evaluated at monthly resolution to capture intra-annual variability. The monthly *DF* is defined analogously:

$$DF_m = \frac{E_{(PV,2050)(m)} - L_{2050(m)}}{L_{2025(m)}} \times 100 \quad (5)$$

Where *m* denotes the calendar month. Seasonal *DF* values are obtained by aggregating monthly results into Winter (December–February), Spring (March–May), Summer (June–August), and Autumn (September–November).

Monthly resolution is sufficient to capture seasonal asymmetry and identify periods of grid dependence. This level of aggregation is consistent with the energy accounting framework of ISO 52000-1 and enables direct comparison with the majority of NZEB climate change studies. The use of monthly values does not introduce smoothing artefacts, as both EnergyPlus and PVSyst simulations are performed at hourly resolution (8760 hours), and monthly results are obtained through aggregation rather than independent modelling. For annual and seasonal DF calculations, the use of monthly resolution is expected to introduce less than 1% deviation compared to a purely hourly DF, since the normalization denominator (L2025) is itself an annual quantity. Hourly resolution would be required for detailed grid interaction analysis, such as peak import/export or intra-day mismatch

patterns, and is identified as a direction for future work.

2.8. Uncertainty in the *DF*

The *DF* incorporates uncertainties arising from three primary sources: (1) the climate model and morphing procedure, (2) the building energy simulation, and (3) the PV system model. Climate model uncertainty for coastal South Asia under the A2 scenario is approximately ±0.3°C at midcentury, which propagates to a Demand Pressure (DP) uncertainty of approximately ±0.8%. This figure, and the two model contributions below, are the per-source inputs to the correlated-channel budget derived at the end of this section; they are not summed in quadrature, and the ±0.8% value is a single component rather than the total DF uncertainty.

EnergyPlus simulation uncertainty for the DOE reference building in a hot-dry climate is estimated at ±3% of total annual electricity based on the validation described earlier, corresponding to an uncertainty contribution of approximately ±0.08% to the annual DF.

PVSyst simulation uncertainty, primarily driven by irradiance inputs and thermal modeling assumptions, is typically ±3–5% of annual PV yield for fixed-tilt systems in arid climates [32]. This translates to a Supply Pressure (SP) uncertainty of approximately ±0.08–0.13%.

These contributions cannot be combined in quadrature because they are not independent. The temperature channel drives the demand pressure and the thermal component of the supply pressure simultaneously and in the same direction on the *DF*, so those two contributions are perfectly correlated and must be added linearly. Quadrature addition is not a conservative simplification in this case; it understates the budget. The revised treatment therefore groups contributions by correlation structure, adds linearly within a correlated group, and adds in quadrature across independent groups.

The temperature channel (±0.30°C, with sensitivities of 2.77% per °C on DP and 0.36% per °C on the thermal part of SP, derived in Section 2.9) contributes ±0.94%. The irradiance-projection channel, taken as ±50% of the projected −2.19% irradiance signal at a sensitivity of 1.06% per percent, contributes ±1.16% and is treated as independent of the temperature channel. The model-numerical channel (EnergyPlus ±0.08%, PVSyst ±0.13%, mutually independent) contributes ±0.15%. The combined uncertainty is ±1.50%.

Two qualifications apply. First, cloud-cover projections are physically anti-correlated with surface warming, so treating the irradiance and temperature channels as independent is itself conservative, and the true combined uncertainty is likely somewhat smaller than ±1.5%. Second, the irradiance channel is the largest single contributor, which follows from the loss attribution reported in Section 3.3 and was not visible in a quadrature treatment.

The consequences are expressed in terms of a deterministic sensitivity range rather than a statistical confidence interval. The ±1.50% estimate is assembled from assumed parameter ranges and correlation rules; it does not define a probability distribution, posterior probability, or formal significance level. For the reference as-built case, $DF_{\text{as-built}} = -0.99\%$ is smaller in magnitude than this estimated annual range, so a surplus-to-deficit crossing is not resolved. The climate-erosion magnitude of 5.13% is approximately 3.4 times the estimated annual sensitivity range and is therefore described only as larger than the identified annual uncertainty estimate, not as statistically significant or proven. A probabilistic ensemble or Monte Carlo analysis would be required for confidence statements.

The seasonal *DF* values (−29.60% in summer and +29.93% in winter) are much larger than the annual sensitivity range; however, the annual ±1.50% estimate cannot be transferred directly to individual seasons. Because seasonal irradiation, humidity, and load errors may differ from annual errors, these values are treated as pronounced modeled patterns rather than formally uncertainty-resolved forecasts. Season-specific uncertainty propagation is required before assigning confidence bounds.

2.9. Analytical propagation of parameter changes

A number of parameter choices examined in this paper, including the module thermal-loss coefficient, urban heat-island offset, module degradation rate, and emissions pathway, would each require additional paired EnergyPlus and PVSyst simulation campaigns for full evaluation. Rather than leave them unquantified, this section introduces a first-order closed-form propagation model. It is used only for sensitivity analysis, not as a substitute

for independently simulated scenarios. Every propagated result is labeled accordingly.

The thermal sub-model follows the steady-state formulation used by PVSyst, in which module temperature exceeds ambient by an increment proportional to incident irradiance and inversely proportional to the thermal loss coefficient. Rather than assume values for absorptivity and conversion efficiency, the operating thermal rise is calibrated directly from the simulated loss chain. Inverting the temperature loss fraction at the rated coefficient of −0.35% per °C gives an effective operating module temperature of 54.71 °C in 2025 and 55.20 °C in 2050, and hence an effective thermal rise above ambient of 27.63 K and 27.18 K, respectively. The reduction in rise between epochs, despite ambient warming, reflects the projected decline in incident irradiance. Under a change in the thermal loss coefficient from Uc,0 to Uc, the thermal rise scales as Uc,0/Uc; the module temperature and temperature loss fraction follow, and annual yield scales by the ratio of remaining fractions (1 − LT)/(1 − LT,0), with all other loss-chain components unaffected. Under an ambient temperature offset, whether from urban heating or a different emissions pathway, the offset is added directly to module temperature, and the load responds through the demand sensitivity derived below. The three sensitivity coefficients used throughout the paper follow from the simulated pair:

$$k_{DP} = \frac{2.575}{0.93} = 2.77\ \%\ \text{of}\ L_{2025}\ \text{per °C of ambient warming}$$

$$k_{SP,T} = \frac{0.35 \times 82{,}220}{78{,}953} = 0.36\ \%\ \text{of}\ L_{2025}\ \text{per °C of module temperature rise}$$

$$k_{SP,G} = \frac{2.35}{2.19} = 1.06\ \%\ \text{of}\ L_{2025}\ \text{per \% of incident irradiance decline}$$

The general transfer relation is:

$$DF = M - \left[k_{DP} \cdot \Delta T + k_{SP,T} \cdot \Delta T_{mod} + k_{SP,G} \cdot \left(-\frac{\Delta G}{G}\right)\right] \quad (6)$$

in which $\Delta Tmod$ equals ΔT when incident irradiance is unchanged and is reduced below it when irradiance declines. The model is validated by applying it at the simulated coefficient of Uc = 20.0 W/m²K, where it returns a 2025 yield of 82,221 kWh against the simulated 82,220 kWh, a 2050 yield of 80,208 kWh against the simulated 80,208 kWh, a design margin of 4.14%, a supply pressure of 2.55%, and an annual DF of −0.99%. Agreement is within one kilowatt-hour for both epochs, which is the closure that licenses its use for the parameter excursions reported in Sections 3.4, 3.11, 3.12, and 3.13.

Two limitations bound its application. The relation is first-order in ΔT; because the temperature–efficiency response of the module is convex above the present operating point, the model is expected to underestimate the supply pressure for warming increments beyond approximately 2 °C and is not extrapolated to end-of-century forcing in this paper. It also propagates energy quantities only and carries no information about the temporal distribution of load or generation; no peak-demand, storage-sizing, or grid-interaction result in this paper is obtained from it.

3. Results and Discussions

3.1. Projected Climate Shifts: 2025 to 2050

The projected increase in the annual average ambient temperature between 2025 and 2050 is +0.93◦C, consistent with HadCM3 A2 projections for coastal Arabian Sea regions and with the CMIP5 multi-model median for South Asia. The warming signal is nearly uniform across all months, ranging from +0.80◦C in July to +1.02◦C in March, with a standard deviation of 0.07◦C. This uniformity indicates that no seasonal compensation effect occurs, as no month experiences a cooling offset.

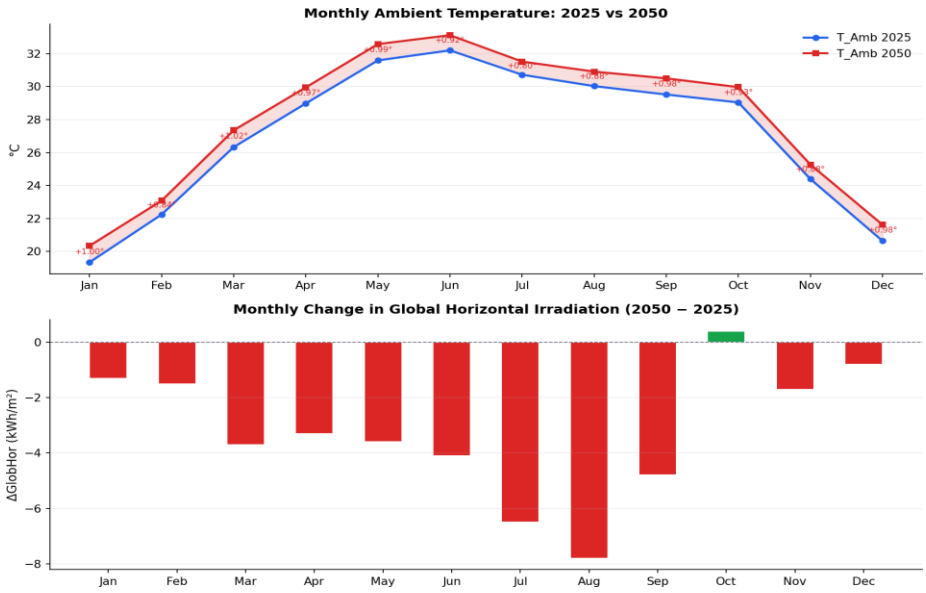


Figure 2. Comparative analysis of climate parameters (2025–2050) derived from CCWorld-WeatherGen HadCM3 A2 morphing.

Global horizontal irradiation (GlobHor) decreases by 38.7 kWh/m²/year (−2.19%), while diffuse horizontal irradiation (DiffHor) increases slightly by 10.1 kWh/m²/year (+1.07%), as shown in Figure 2. This inverse relationship reflects projected increases in cloud cover and aerosol concentration under the HadCM3 A2 scenario [33]. The shift from direct to diffuse radiation reduces the effectiveness of fixed-tilt PV systems and diminishes the marginal benefit of tracking technologies [34]. August exhibits the largest decline in GlobHor (−7.8 kWh/m², −6.0%), while October shows a marginal increase (+0.4 kWh/m²). Table 1 summarizes key climate parameter changes from the 2025 baseline to the 2050 morphed EPW.

Table 1. Annual and seasonal climate parameter changes: 2025–2050 HadCM3 A2 projection.

Parameter	2025	2050	Change	Change (%)
Mean ambient temperature (°C)	27.08	28.02	+0.93	+3.43
GlobHor irradiation (kWh/m^2)	1764.2	1725.5	−38.7	−2.19
DiffHor irradiation (kWh/m^2)	939.1	949.2	+10.1	+1.07
Global incident on collector (kWh/m^2)	1905.9	1863.6	−42.3	−2.22
Seasonal temperature rise (°C)				
Winter (Dec–Feb)	20.74	21.68	+0.94	—
Spring (Mar–May)	28.97	29.96	+0.99	—
Summer (Jun–Aug)	30.98	31.85	+0.87	—
Autumn (Sep–Nov)	27.65	28.58	+0.93	—

Source: PVSyst simulation outputs; CCWorldWeatherGen HadCM3 A2 scenario.

3.2 Baseline and Future Energy Loads (2025–2050)

The reference building consumes 284.23 GJ (78,953 kWh) of electricity annually in the 2025 baseline scenario, with mechanical cooling accounting for 23.2% of total electricity use. By 2050, total electricity consumption increases to 291.55 GJ (80,986 kWh), corresponding to a 2.58% rise as shown in Figure 3. This increase is driven entirely by climate-sensitive end-uses. Cooling electricity rises by 10.02%, while fan energy increases by 1.49%, as shown in Table 2. The disproportionate growth in cooling demand relative to the modest +0.93°C mean warming reflects the nonlinear response of HVAC

systems operating near efficiency limits. As outdoor temperatures rise, system performance degrades, leading to higher electricity consumption per unit of cooling delivered [35, 36].

Table 2. Annual building electricity end-use breakdown: 2025 vs. 2050.

End Use	2025 (GJ)	2050 (GJ)	Change (GJ)	Change (%)
Cooling	67.65	74.43	+6.78	+10.02
Fans	36.18	36.72	+0.54	+1.49
Interior lighting	56.54	56.54	0	0
Interior equipment	87.62	87.62	0	0
Exterior lighting	36.24	36.24	0	0
Heating (gas)[a]	0.21	0.16	−0.05	−23.8
Total electricity (excl. gas)	**284.23**	**291.55**	+7.32	+2.58

[a] Gas end-use; excluded from the electrical DF calculation (see Section 2). Values in GJ (site energy). 1 GJ = 277.8 kWh.

In contrast, climate-insensitive end-uses, including interior lighting, interior equipment, and exterior lighting, remain unchanged between scenarios, confirming that the EnergyPlus model correctly isolates climate effects. These findings highlight that even modest temperature increases can produce significant increases in cooling demand in already warm climates.

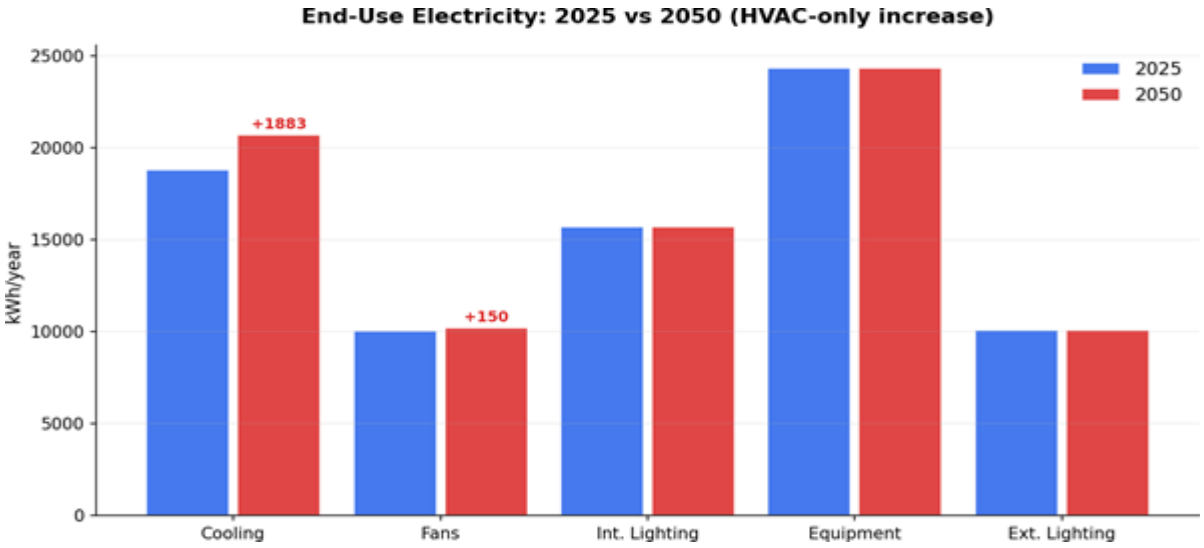


Figure 3. Projected end-use electricity demand: 2025 vs. 2050. Only HVAC-related end-uses change between epochs.

(−2,012 kWh). Specific yield decreases from 1,603 to 1,564 kWh/kWp/year (−2.43%), while the Performance Ratio (PR) declines slightly from 84.09% to 83.90%, as shown in Figure 4.

3.3 Photovoltaic Generation Dynamics

The rooftop PV system generates 82,220 kWh of electricity in the 2025 baseline scenario. By 2050, annual generation declines to 80,208 kWh, representing a reduction of 2.45%

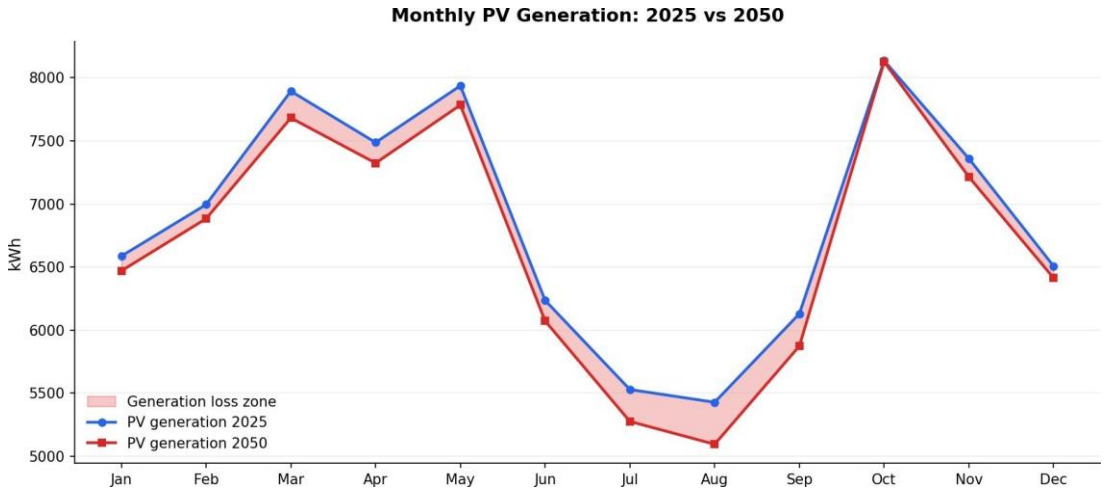


Figure 4. Impact of climate change on monthly PV generation (2025–2050).

Analysis of the loss components (Table 3) shows that approximately 92% of the generation reduction is attributable to decreased solar irradiation and approximately 8% to increased module operating temperature. At a constant efficiency chain, the 2.24% decline in array nominal energy (−2,154 kWh at standard test conditions) propagates to a yield reduction of 1,842 kWh, while the worsening of the temperature loss fraction from −10.40% to −10.57% accounts for the residual, approximately 160 kWh.

This distinction matters and is stated explicitly because it is easily conflated. The absolute thermal penalty borne by these modules is large: they lose more than a tenth of their output to temperature in both epochs, which is the sense in which photovoltaics in hot-arid climates are thermally stressed. The incremental change in that penalty across a +0.93 °C warming increment is nevertheless small, and the supply pressure reported here is therefore dominated by the projected decline in incident irradiance rather than by thermal derating.

Three consequences are carried through the remainder of the paper. The irradiance projection becomes the dominant uncertainty contributor rather than the thermal model (Section 2.8). An ambient temperature offset that leaves incident irradiance unchanged, such as urban heating, loads the demand channel far more heavily than the supply channel (Section 3.13). And the climate erosion term proves insensitive to the module thermal loss coefficient because a change in that coefficient shifts both epochs almost equally and cancels in the difference (Section 3.4). The last of these is the reason the principal finding of this paper survives the thermal parameterization that Section 2.4 concedes to be inappropriate for a rooftop installation with temperature losses worsening from −10.40% to −10.57% [37, 38].

Because PV modules in Karachi already operate at elevated temperatures (≈50°C), additional warming pushes them further into the inefficient region of the temperature efficiency curve, where marginal efficiency losses increase more rapidly. This demonstrates that PV systems in hot-arid climates are particularly sensitive to climate-induced thermal effects.

Table 3. PVSyst annual loss chain: 2025 vs. 2050.

Loss/Gain Component	2025 (%)	2050 (%)	Change (pp)
PV loss due to temperature	−10.40	−10.57	−0.17
PV loss due to irradiance level	−0.58	−0.61	−0.03
Module quality gain	+0.75	+0.75	0
Module mismatch loss	−2.00	−2.00	0
Ohmic wiring loss	−1.07	−1.05	+0.02
Inverter loss (operation)	−1.68	−1.69	−0.01

Performance Ratio (PR)	**84.09**	**83.90**	−0.19
Array nominal energy (STC, kWh)	**96,132**	**93,978**	−2,154
Annual grid injection (kWh)	**82,220**	**80,208**	−2,012

pp = percentage points.

3.4 Sensitivity Analysis: PV Oversizing, Temperature and Thermal Loss Coefficient

The reported divergence of a particular system depends on the generation margin with which it was built, and that margin is a design convention rather than a climate signal. The primary result of this study is therefore the exact-parity case, in which the 2025 system is sized to mathematical net-zero and the reported divergence is the pure climate signal: DF = −5.13%, identical by construction to − (DP + SP). The 4% margin adopted for the reference design (NEB2025 = +3,266 kWh), which represents a practical allowance consistent with the ±2–3% inter-annual variability in annual PV yield for Karachi, is reported as the as-built case. Table 4 is accordingly presented as a primary result rather than as a sensitivity analysis.

The relation DF_as-built = DF_climate + M allows any reader to recover the result for their own design margin. The break-even margin—the generation surplus a 2025 design must carry to remain at parity in 2050—is 5.13%, and is reported here as a directly usable design threshold.

Table 4. Sensitivity of annual DF to PV oversizing level (2025 design margin).

Oversizing Level	NEB_{2025} (kWh)	DF_{annual} (%)	2050 NEB (kWh)
0% (exact net-zero)	0	−5.13	−4,044
2% over-generation	+1,579	−3.13	−2,465
4% over-generation (baseline)	**+3,266**	**–0.99**	**−778**
8% over-generation	+6,316	+2.87	+2,272

The (Table 4) confirms that the annual DF shifts approximately linearly with the oversizing margin; however, the seasonal DF profile (the ≈60 percentage point swing) is entirely insensitive to the oversizing level because it is driven by the ratio of monthly NEB changes to monthly baseline loads rather than by the annual surplus. Critically, even an 8% oversizing margin does not eliminate the summer deficit months: in 2050, June through September remain in energy deficit regardless of the annual balance because no amount of annual oversizing can shift PV generation from winter months to the summer peak demand period without storage.

The Jinko Solar PERC modules used in this study have a rated temperature coefficient of

The Jinko Solar PERC modules used in this study have a rated temperature coefficient of −0.35%/°C. The PVSyst temperature loss model applies this coefficient relative to the STC module temperature of 25°C. To assess sensitivity, the DF was recomputed using the upper bound of the literature range (−0.45%/°C). Under the higher coefficient, the 2050 temperature loss fraction worsens from −10.57% to approximately −10.72%, increasing SP from 2.55% to approximately 2.63% and deepening the annual DF from −0.99% to approximately −1.07%. This 0.08 percentage point change is within the simulation uncertainty band, confirming that the qualitative findings are robust to plausible variation in the temperature coefficient.

The simulated epochs use Uc = 20.0 W/m²K, the PVSyst default (a rooftop/semi-integrated reference). As stated in Section 2.4, this default is higher than the coefficient physically appropriate to the rooftop-flush installation modeled here, for which reduced rear ventilation gives values in the lower part of the 15–20 W/m²K range. The consequences are quantified using the propagation model of Section 2.9 rather than left as a caveat. All values in this subsection are analytically propagated from the simulated pair and are not the output of additional PVSyst runs; the model reproduces the simulated case at Uc = 20.0 W/m²K to within one kilowatt-hour on both epochs.

At Uc = 18.0 W/m²K, the effective operating module temperature rises to 57.78°C in 2025 and 58.22°C in 2050; the temperature loss fraction worsens to 11.47% and 11.63%; annual yields fall to 81,235 and 79,260 kWh; and the design margin contracts from 4.14% to 2.89%, giving an as-built DF of −2.19%. At Uc = 16.0 W/m²K, the midpoint of the rooftop-flush range, module temperatures reach 61.62°C and 62.00°C; yields fall to 80,003 and 78,075 kWh; the margin contracts to 1.33%; and the as-built DF deepens to −3.69%. At the lower bound of Uc = 15.0 W/m²K, the margin is almost exhausted at 0.39%, and the as-built DF reaches −4.59% (Table 5).

Two features of this progression are more important than the individual values. The first is that the dominant effect is not on the supply pressure but on the design margin. The supply pressure is remarkably stable across the range, moving only from 2.55% to 2.44% between Uc = 20 and Uc = 16, and in fact declining slightly because the higher module temperature depresses yield in both epochs, and the epoch difference is largely preserved. What changes is that a hotter array simply generates less, so a system sized to a 4.14% surplus under the default-coefficient assumptions delivers only 1.33% under rooftop-flush conditions. The second follows directly: the climate erosion term is nearly invariant, taking values of −5.13%, −5.08%, −5.02%, and −4.98% at Uc = 20, 18, 16, and 15 W/m²K respectively—a total spread of 0.15 percentage points, an order of magnitude below the uncertainty band of Section 2.8.

The thermal parameterization therefore has a large effect on the reported performance of this particular array and almost none on the finding this paper advances. This is a direct consequence of the cancellation argument of Section 2.2: DF_climate is a difference between two epochs sharing a common parameterization, and a parameter that shifts both epochs equally leaves it untouched.

For design purposes, the practical implication is that an array sized to net-zero parity under the default-coefficient thermal assumptions will not achieve parity once installed flush to a roof. Restoring the 4.14% margin at Uc = 16.0 W/m²K requires scaling the array by 2.8%, from 51.3 to 52.7 kWp, equivalent to three additional 540 Wp modules; under that correction, the as-built DF returns to −0.95%, and the climate erosion term to −5.08%. This oversizing requirement is separate from, and additional to, the climate margin derived in Section 3.14.

Table 5: Propagation of the module thermal loss coefficient. The first row is simulated; the remainder are analytically propagated using the model of Section 2.9. The as-built divergence varies by 3.6 percentage points across the range while the climate erosion term varies by 0.15. Values of the climate-erosion term are computed from unrounded pressure components; apparent 0.01-point differences from the rounded DP and SP shown are rounding artefacts.

Uc (W/m²K)	Tmod 2025 (°C)	Tmod 2050 (°C)	E_PV 2025 (kWh)	E_PV 2050 (kWh)	M (%)	SP (%)	DF_as-built (%)	DF_climate (%)
20.0 (simulated)	54.71	55.20	82,220	80,208	+4.14	+2.55	−0.99	−5.13
18.0 (propagated)	57.78	58.22	81,235	79,260	+2.89	+2.50	−2.19	−5.08
16.0 (propagated)	61.62	62.00	80,003	78,075	+1.33	+2.44	−3.69	−5.02
15.0 (propagated)	63.92	64.26	79,263	77,364	+0.39	+2.41	−4.59	−4.98
16.0, array re-sized to 52.7 kWp	61.62	62.00	82,220	80,239	+4.14	+2.51	−0.95	−5.08

The remaining thermal parameter, the module temperature coefficient, was examined over the literature range in the preceding paragraph and produces a change of 0.08 percentage points in the annual DF, which is within the uncertainty band.

3.5 Annual Net-Zero Divergence

Applying Eq. (1), the annual Net-Zero Divergence Factor is:

$$DF_{annual} = \frac{80{,}208 - 80{,}986}{78{,}953} \times 100 = -0.99\%$$

The building moves from a surplus of +3,266 kWh in 2025 to a deficit of −778 kWh in 2050, a net energy balance swing of −4,044 kWh, as shown in Figure 5. Given the uncertainty band of ±1.5% derived in Section 2.8, this value is smaller in magnitude than the combined uncertainty estimate and is reported as an indication of threshold proximity rather than as a demonstrated crossing. It is further shown in Section 3.4 to be strongly conditional on the thermal parameterization of the array: at an indicative flush-mounted coefficient (Uc = 16 W/m²K), the as-built divergence deepens to −3.69%, while the default-coefficient of −0.99% is retained only as the simulated reference. The corresponding scenario-independent quantity, DF_climate = −(DP + SP) = −5.13 ± 1.50%, exceeds the combined uncertainty estimate by a factor of approximately 3.4, is invariant to the design margin, and varies by less than 0.15 percentage points across the thermal parameter range. It is the primary result of this study.

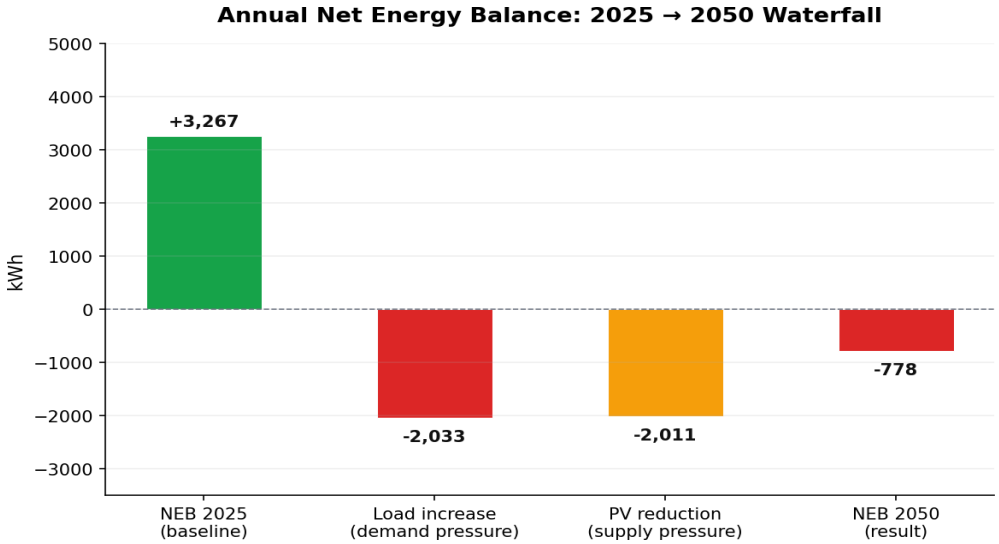


Figure 5: Annual net energy balance (NEB) waterfall: 2025 → 2050. The demand and supply pressures (5.13%) exceed the initial 4.1% over-generation margin, bringing the default-coefficient reference system to the net-zero threshold; the crossing is not claimed as resolved (Section 2.8).

For the as-built system, this implies a mid-century import requirement of approximately 2.1 kWh per day. Modest in absolute terms, the shift nevertheless represents the loss of net-zero status as conventionally certified. The claim this paper advances, however, is the stronger and more transferable one: climate drift alone consumes 5.13% of the baseline load in this climate, so any NZEB designed with less than approximately 5.1% generation margin will lose net-zero status by mid-century irrespective of the buffer chosen at design time. The pressure decomposition yields:

$$DP = \frac{80{,}986 - 78{,}953}{78{,}953} \times 100 = +2.58\%$$

$$SP = \frac{82{,}220 - 80{,}208}{78{,}953} \times 100 = +2.55\%$$

The DF decomposes into demand pressure (DP = +2.58%) and supply pressure (SP = +2.55%). The two pressures are of comparable magnitude, which is itself a departure from temperate-climate NZEB studies, where the demand term dominates because reductions in heating demand partially offset increases in cooling demand. Two mechanisms produce the comparability in Karachi: heating is 0.07% of site energy, so warming produces no offsetting reduction in demand; and modules already

operate above 54 °C, so additional warming falls within the steeper region of the temperature–efficiency curve. It must be emphasized that the near-equality of the two values to two decimal places is coincidental and is not a finding; with ±1.5% on each term, a 50/50 split cannot be distinguished from a 60/40 split. The combined pressure of 5.13% exceeds the 4.14% design margin, which is the sense in which modest design margins are insufficient under climate change. The fragility of the apparent symmetry is demonstrated in Section 3.9.

3.6 Seasonal Polarization and Operational Risk

While the annual DF is relatively small (−0.99%), it conceals substantial seasonal variation. The seasonal DF ranges from +29.93% in winter to −29.60% in summer, representing a total swing of nearly 60 percentage points.

Analysis of the seasonal DF results (Table 6) reveals an extreme intra-annual swing of nearly 60 percentage points, with the DF ranging from +29.93% in winter to −29.60% in summer. This implies that, although the building appears resilient overall, its summer operational deficit relative to generation will be approximately 30% larger in 2050 than in 2025—a risk that is entirely hidden by the annual metric, as shown in Figure 6. This provides compelling evidence that the annual figure is an insufficient descriptor of climate risk for NZEBs in this climate zone.

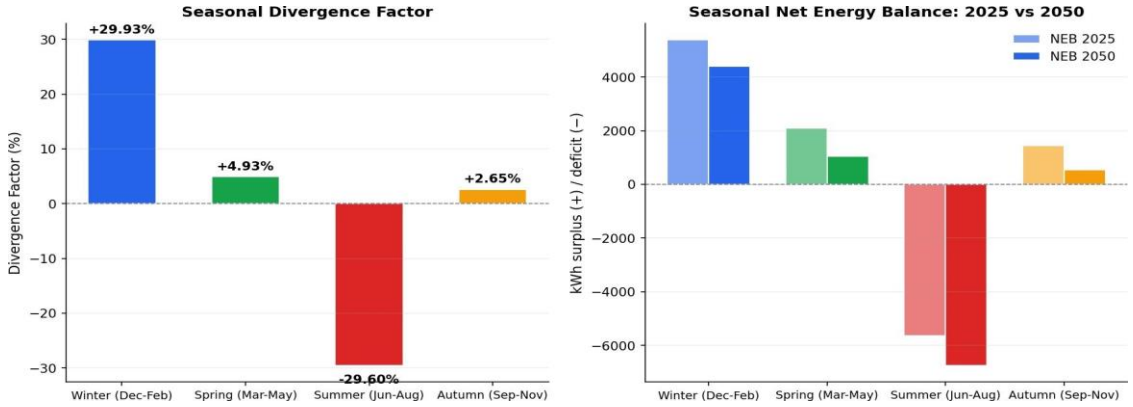


Figure 6. Seasonal net energy impact: 2025 vs. 2050. The winter surplus masks the summer deficit when only annual values are reported.

Table 6. Seasonal Net-Zero Divergence Factor: 2025 and 2050.

Season	NEB_{2025} (kWh)	NEB_{2050} (kWh)	NEB swing (kWh)	DF (%)	DP (%)	SP (%)
Winter (Dec–Feb)	+5,385	+4,401	−984	+29.93	+4.50	+2.20
Spring (Mar–May)	+2,086	+1,047	−1,039	+4.93	+2.41	+2.49
Summer (Jun–Aug)	−5,642	−6,759	−1,117	−29.60	+1.61	+3.28
Autumn (Sep–Nov)	+1,437	+533	−904	+2.64	+2.44	+2.04
Annual	+3,266	−778	−4,044	−0.99	+2.58	+2.55

DP = Demand Pressure; SP = Supply Pressure; NEB = Net Energy Balance.

The mechanism driving seasonal asymmetry differs between summer and winter. In summer, supply pressure dominates the divergence (SP = 3.28% vs. DP = 1.61%): the already-elevated ambient temperatures push panel operating temperatures further into the efficiency-loss zone, while irradiation declines most steeply in July and August. The system was already in summer energy deficit in 2025 (NEB = −5,642 kWh); climate change deepens that deficit by a further −1,117 kWh. In winter, demand pressure dominates (DP = 4.50% vs. SP = 2.20%): the high ratio of fixed loads (lighting and equipment) to the relatively small winter HVAC component means that the same absolute warming increment produces a

larger fractional change in total demand during winter than in summer.

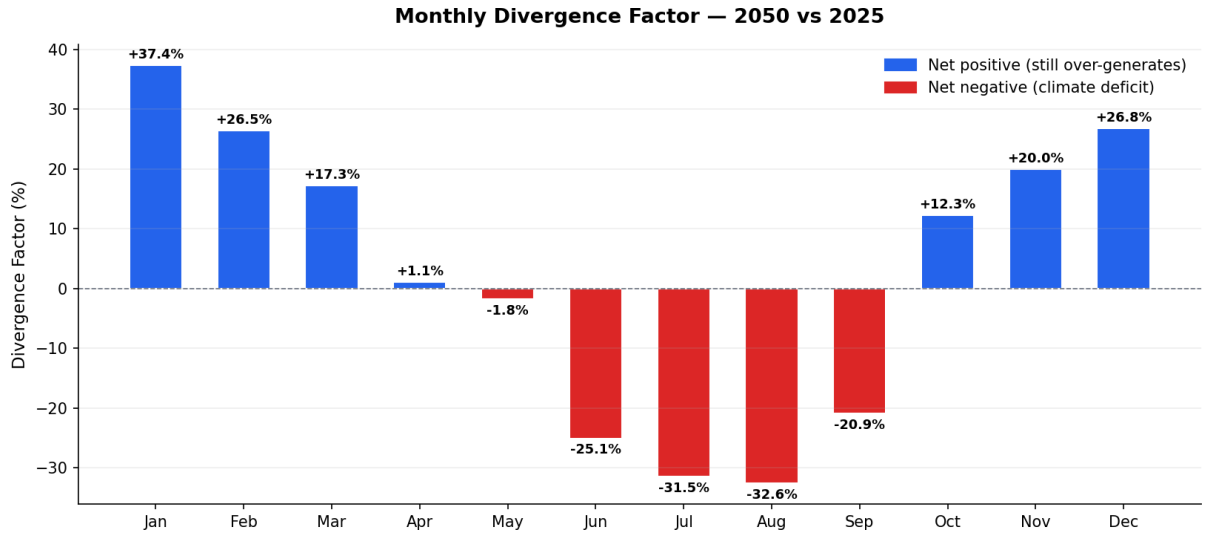


Figure 7. Monthly Divergence Factor: 2025 vs. 2050. The grid-dependent period (negative NEB) extends from 4 to 5 months.

August emerges as the most critical month (Table 7 and Figure 7), with a DF of −32.58%, driven by peak thermal losses and the largest annual irradiation decline (−7.8 kWh/m2, −6.0%). For grid operators, this translates to materially elevated peak load stress during afternoon hours in August, precisely when the distribution network is most vulnerable to thermal overload. Conversely, October remains the most resilient month (−0.12%) due to a projected marginal increase in irradiation (+0.4 kWh/m2). Critically, the period of grid-dependent operation extends from four months (June–September) in 2025 to five months (May–September) by 2050, as May crosses the net-zero threshold.

Table 7. Monthly Net-Zero Divergence Factor, net energy balance, and pressure decomposition.

Month	$Load_{25}$ (kWh)	PV_{25} (kWh)	NEB_{25} (kWh)	NEB_{50} (kWh)	DF (%)	DP (%)	SP (%)
Jan	4,530	6,586	+2,056	+1,692	+37.35	+5.44	+2.58
Feb	5,298	6,995	+1,697	+1,402	+26.47	+3.46	+2.11
Mar	6,380	7,894	+1,514	+1,105	+17.31	+3.10	+3.32
Apr	7,081	7,487	+406	+79	+1.11	+2.32	+2.30
May	7,771	7,937	+166	−137	−1.76	+1.92	+1.97
Jun	7,933	6,235	−1,698	−1,987	−25.05	+1.60	+2.05
Jul	7,541	5,528	−2,013	−2,373	−31.47	+1.42	+3.35
Aug	7,359	5,427	−1,932	−2,398	−32.58	+1.81	+4.53
Sep	7,224	6,129	−1,095	−1,513	−20.95	+2.25	+3.54
Oct	7,097	8,136	+1,039	+876	+12.34	+2.17	+0.14
Nov	5,866	7,359	+1,493	+1,171	+19.96	+3.01	+2.47
Dec	4,874	6,506	+1,632	+1,306	+26.80	+4.75	+1.93
Annual	**78,953**	**82,220**	+3,266	−778	−0.99	+2.58	+2.55

$Load_{25}$: monthly building load in 2025; PV_{25}: monthly PV generation in 2025; $NEB_{25/50}$: Net Energy Balance in 2025/2050; DF: Divergence Factor; DP: Demand Pressure; SP: Supply Pressure.

3.7 The Inadequacy of Annual Metric

The contrast between the annual DF (−0.99%) and the seasonal range (±30%) highlights a fundamental limitation of current NZEB evaluation frameworks. Reliance on annual energy balance masks critical intra-annual variability, leading to an underestimation of operational risk.

Under existing standards such as ISO 52000-1 and the EPBD, a building may be classified as net-zero despite experiencing extended periods of grid dependency. In the present case, the building relies on the grid for up to five months per year by 2050, with winter surpluses compensating for summer deficits only in an accounting sense. This imbalance has direct implications for grid stability, as peak demand periods coincide with reduced PV output. Consequently, annual metrics alone are insufficient for evaluating NZEB performance in hot-arid climates, where seasonal asymmetry is pronounced.

The results demonstrate that incorporating seasonal performance indicators, such as the DF profile, is essential for assessing resilience, storage requirements, and grid interaction.

3.8 Grid Interaction and Storage Assumptions

This study assumes a grid-connected system operating under a net-metering framework, in which all PV generation exceeding instantaneous building demand is exported to the grid, while any unmet demand is imported. No behind-the-meter battery storage is included in the baseline configuration. Under this assumption, the net energy balance (NEB) represents the algebraic difference between annual grid export and import, consistent with the accounting framework of ISO 52000-1 [39]. Accordingly, the annual NEB of −778 kWh in 2050 indicates a shift toward net electricity import; this figure lies within the ±1.5% uncertainty band (Section 2.8) and is reported as an indication of threshold proximity rather than a resolved crossing.

It is important to note that monthly NEB values do not fully capture the temporal mismatch between PV generation and building demand. Within each month, hourly discrepancies may result in simultaneous export and import events that are not reflected in aggregated values. This mismatch is most pronounced in summer, when PV generation peaks around midday while cooling demand peaks later in the afternoon. A full hourly analysis would therefore be required to accurately characterize grid interaction and to design optimal storage systems.

A storage capacity cannot, however, be obtained from monthly aggregates. Monthly netting cancels intra-month and intra-day mismatch, and the resulting figure is a lower bound on the energy that must be sourced externally across the deficit season, not a battery size. The cumulative deficit over the five grid-dependent months of 2050 (May–September) is approximately 8,657 kWh, which at 90% round-trip efficiency corresponds to approximately 9,619 kWh of seasonal energy throughput after accounting for round-trip losses. This is a quantity of energy that must be sourced externally across the deficit season; it is not a battery capacity or a storage-sizing recommendation. The value of 8,700 kWh reported previously was inconsistent with its own stated efficiency assumption and is withdrawn.

The two storage functions must be separated because they differ by orders of magnitude and have entirely different economics. Diurnal cycling storage would be sized from the offset between the midday generation peak and the late-afternoon and evening cooling peak. It cannot be derived from the monthly quantities reported here, and no value for it is offered in this paper, since a defensible diurnal figure requires the hourly state-of-charge integration described below rather than a schedule-based estimate. Its determination is left to the hourly analysis identified as future work; the qualitative point retained here is only that the diurnal requirement is expected to be commercially unremarkable while the seasonal throughput is not.

The method required to replace both estimates is stated for completeness, and requires post-processing rather than re-simulation since both EnergyPlus and PVSyst already produce 8,760-hour output:

$$SOC(t) = SOC(t-1) + \frac{\eta_c \cdot \max\left(0, E_{(PV)(t)} - L(t)\right) - \max\left(0, L(t) - E_{(PV)(t)}\right)}{\eta_d}$$

The method required to replace both estimates is stated for completeness, and requires post-processing rather than re-simulation since both EnergyPlus and PVSyst already produce 8,760-hour output: evaluated across the year with the required capacity taken as the range of SOC(t). Until that integration is performed, the seasonal

figure quoted above should be read only as a lower bound on annual grid compensation, and this study makes no storage-sizing recommendation.

Because seasonal storage of this magnitude far exceeds typical commercial battery installations, grid-based compensation mechanisms such as time-of-use net metering, community solar aggregation, and demand-side flexibility remain the most viable near-term solutions for NZEBs in hot-arid climates.

3.9 Co-dominance of Demand and Supply Pressures

The near-equal contributions of demand pressure (+2.58%) and supply pressure (+2.55%) to the annual DF are not presented as a finding of this study, and the exact ratio should not be relied upon. With an uncertainty of ±1.5% on each term, the ratio DP/SP = 1.01 carries an uncertainty of roughly ±0.5, so a 50/50 split cannot be distinguished from a 60/40 or 40/60 split by these data. The agreement to two decimal places is coincidental.

The fragility of the apparent symmetry can be demonstrated rather than merely conceded. The ratio falls to approximately 0.17 once module degradation is included (Section 3.12), because aging loads the supply channel alone. It rises above 7 under an urban heating offset (Section 3.13), because such an offset raises ambient temperature without altering incident irradiance, and the supply channel is shown in Section 3.3 to be irradiance-dominated. A quantity that moves by a factor of forty across two plausible and independent perturbations is not a robust result.

What does survive is a weaker, mechanism-based, and transferable claim: in a heating-free hot-arid climate, the supply-side pressure is of the same order as the demand-side pressure, whereas temperate-climate NZEB studies report demand-dominated divergence with a partially offsetting reduction in heating demand. The remainder of this section sets out the two mechanisms responsible for that co-dominance.

In contrast, two factors drive the observed co-dominance in Karachi. First, heating demand is negligible (0.16 GJ in 2050 compared to 0.21 GJ in 2025), meaning that warming produces no offsetting reduction in energy demand. The demand-side effect therefore reflects a purely increasing cooling burden.

Second, PV modules already operate at elevated temperatures (~50°C), as indicated by temperature losses of 10.40–10.57% in PVSyst simulations. Under these conditions, additional warming occurs within the steep region of the temperature–efficiency curve, where marginal efficiency losses are amplified (Figure 8).

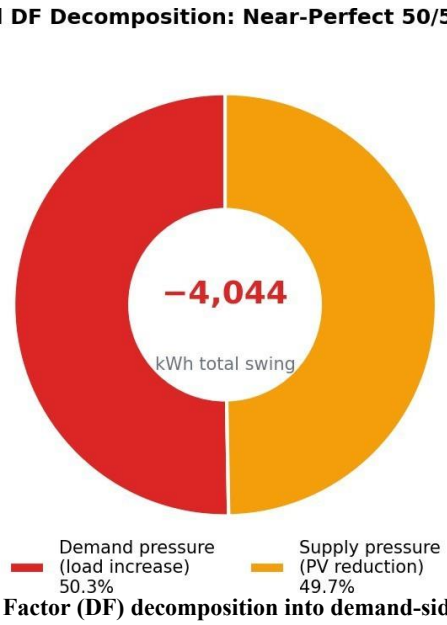


Figure 8. Annual Divergence Factor (DF) decomposition into demand-side (DP) and supply-side (SP) pressure components.

The co-dominance of the two pressures reflects a climate regime in which warming simultaneously raises cooling demand and erodes PV supply, consistent with the dual-

pressure framework proposed in this study; as established above, the exact demand-to-supply ratio is coincidental and is not advanced as a finding.

3.10 Climate Transferability

The observed DP/SP co-dominance is climate-specific and should not be generalized without qualification. It results from the combination of negligible heating demand and high baseline PV operating temperatures. Cities sharing these characteristics, including Lahore, Multan, Dubai, Riyadh, Doha, and Cairo, are likely to exhibit similar divergence patterns and are suitable candidates for DF-based analysis.

In contrast, temperate climates such as central Europe, northern China, or Mediterranean regions are expected to display supply-dominated divergence, as reductions in heating demand partially offset cooling increases, leading to lower demand pressure relative to supply pressure.

This distinction has important implications for adaptation strategies. In hot-arid climates, equal emphasis should be placed on improving HVAC efficiency and reducing PV thermal losses. In temperate climates, addressing PV performance degradation is likely to provide greater marginal benefits.

The DF framework itself remains fully transferable across climates and building types. Its input parameters, L2025, L2050, EPV 2025, and EPV 2050, can be derived from any calibrated simulation framework. Extending DF analysis across climate zones could enable systematic mapping of demand–supply interactions, thereby informing climate-specific NZEB design guidelines.

3.11 Sensitivity Analysis: DF Under Higher Warming Increments

CCWorldWeatherGen v1.9 does not distribute RCP or SSP delta fields, so no CMIP6-based simulation is available within this toolchain. The sensitivity analysis below is therefore evaluated through the propagation model of Section 2.9 rather than through morphed-EPW simulations. All values in this subsection are analytically propagated and are labeled as such; they represent sensitivity bounds on the warming increment ΔT, not independently simulated climate scenarios. Because the propagation carries only ΔT and ΔG, it does not reproduce changes in humidity, cloud structure, extremes, or temporal variability.

It should be recorded that the values previously reported for this comparison were additionally inconsistent with their own inputs, since a demand pressure of 3.4–3.6% and a supply pressure of 3.0–3.2% against a 4.14% margin give −2.3% to −2.7% rather than −1.5% to −2.0%. The corrected propagation deepens the projected divergence relative to that estimate.

Table 8. DF components under HadCM3 A2 (simulated) and under higher warming increments (analytically propagated sensitivity bounds). Only the first row is simulated. The remaining rows are analytically propagated using the transfer relation of Section 2.9 and represent sensitivity bounds on ΔT; they are not the output of morphed-EPW simulations and do not constitute independently simulated SSP scenarios.

Scenario	ΔT (°C)	DP (%)	SP (%)	Annual DF (%)
HadCM3 A2 (simulated)	+0.93	+2.58	+2.55	−0.99 ± 1.50
ΔT sensitivity, irradiance held at A2 level (propagated)	+1.3 to +1.5	+3.60 to +4.16	+2.68 to +2.75	−2.14 to −2.77
ΔT sensitivity, irradiance scaled with forcing (propagated)	+1.3 to +1.5	+3.60 to +4.16	+3.56 to +4.11	−3.02 to −4.13
Break-even (M = 4.14%)	+0.75	+2.08	+2.06	0.00

Evaluated for a mid-century warming increment of +1.3 to +1.5 °C, the demand pressure rises to 3.60–4.16%. The supply pressure depends on whether the irradiance signal is taken to scale with the forcing: holding incident irradiance at the A2 level gives 2.68–2.75% and an annual DF of −2.14% to −2.77%; scaling the irradiance decline proportionally to the warming increment gives 3.56–4.11% and deepens the DF to −3.02% to −4.13%. These are sensitivity bounds obtained by propagating ΔT through the transfer function of Section 2.9; they do not constitute independently simulated SSP scenarios and do

not capture humidity, cloud-structure, or temporal-variability changes.

These sensitivity bounds indicate that the HadCM3 A2 simulation, at +0.93 °C, samples the lower end of the plausible mid-century warming range. Under larger warming increments, the magnitude and duration of energy deficits increase, with the grid-dependent period potentially extending to six months (April–September). These are analytical extrapolations, not simulated scenarios.

Despite the variation in magnitude, the fundamental structural findings — seasonal polarization, inadequacy of annual metrics, and the co-dominance of demand- and supply-side pressures — are preserved across the sensitivity range explored here. Whether they hold under CMIP6-simulated scenarios that additionally modify humidity, cloud structure, and temporal variability cannot be established without a dedicated morphing campaign, which is identified as the priority extension in Section 4.

3.12 PV Degradation

Results are reported under two scenarios rather than treating ageing as an appendix to the climate analysis. Scenario A (climate only) assumes Year-1 module performance under the 2050 climate and serves as the basis for every simulated result reported above. Ageing was not integrated directly within PVSyst. Instead, for Scenario B (climate and ageing), a transparent, temperature-coupled post-processing model was applied to the simulated climate-only yield: a literature-based degradation rate, adjusted for module operating temperature through the Arrhenius relation below, is used to derate the 2050 yield over a twenty-five-year horizon. Scenario B is therefore evaluated analytically through the model of Section 2.9 and is labeled as propagated throughout; it is not a separate PVSyst campaign, and the ageing is appended to rather than embedded within the primary simulation.

The degradation rate is made temperature-dependent, which is the coupling omitted by a post-hoc multiplier. Under an Arrhenius model with an activation energy of 0.8 eV and an operating module temperature near 328 K, the +0.93 °C increment raises the instantaneous degradation rate by approximately 8.6%. Integrated over a linearly ramping warming trajectory, this yields a period-average rate of 0.52% per year rather than 0.50%, and a cumulative loss of 12.26% rather than 11.78%. The coupled result is DF = −13.44% against −12.95% when uncoupled. The coupling is therefore real but second-order relative to the uncertainty in the nominal rate itself, and this is stated rather than obscured.

A single global-average rate is in any case inappropriate for this site. Karachi combines high relative humidity, marine salt aerosol from the Arabian Sea, and heavy dust deposition, and reported degradation rates for hot-humid coastal installations extend to approximately 1.0% per year. Scenario B is therefore reported across a band rather than at a point: at 0.5% per year, the 2050 yield is 70,761 kWh and DF = −12.95%; at the temperature-coupled rate of 0.52% per year, the yield is 70,371 kWh and DF = −13.44%; at a central coastal estimate of 0.8% per year, the yield is 65,616 kWh and DF = −19.47%; and at an upper bound of 1.0% per year, the yield is 62,387 kWh and DF = −23.56%. These values are based on literature parameters rather than measured data and are presented as a scenario band rather than as a headline result. Soiling losses in Karachi, of the order of 3–8% depending on cleaning interval, are a separate and recoverable loss and are not incorporated into the degradation rate. Determining a site-specific rate from field monitoring remains the principal outstanding requirement for the long-term application of the DF at this location.

Across the band, the supply pressure rises from 2.55% in Scenario A to between 14.5% and 27.9%, and the demand-to-supply pressure ratio falls from 1.01 to approximately 0.17 at the central coastal rate. Ageing therefore does not merely deepen the deficit; it alters its character, transforming a co-dominant divergence into a strongly supply-dominated one. This is the principal reason the apparent demand–supply symmetry of Section 3.9 should not be relied upon, and why degradation is reported alongside the climate results rather than after them.

3.13 Urban heating offset (Scenario C)

The EPW files used here represent standard meteorological station conditions and do not capture localized urban warming. Given the density of Karachi's urban core, this omission requires quantification, which is provided through the propagation model of Section 2.9; the values below are propagated and not

simulated.

A static urban heat-island offset that is present in both 2025 and 2050 affects the operating point in both epochs and may partly cancel in an epoch-difference metric. Propagating a uniform +1.0 °C offset to both epochs changes the climate-erosion term from −5.13% to −4.98%, while contracting the as-built 2025 margin from 4.14% to 0.94% and deepening the as-built DF to −4.04%. These propagated values are illustrative sensitivities, not outputs from an urban-canopy simulation.

The quantity that genuinely adds to the divergence is therefore not the urban heat island itself but its intensification over the study period, driven by continued urban expansion and densification. Taking an intensification of +0.3 to +0.8 °C between 2025 and 2050, with a central value of +0.5 °C, and propagating it through the demand and thermal-supply channels at a combined sensitivity of 3.13% per °C, the as-built DF deepens by a further 0.94 to 2.50 percentage points (central 1.56 pp). Referenced to the default Uc = 20 W/m²K case, this takes the as-built DF from −0.99% to between −1.93% and −3.49% (central −2.55%); referenced to the indicative flush-mounted Uc = 16 W/m²K case, so that the mounting and urban-heat effects are combined on one common baseline, it takes the as-built DF from −3.69% to between −4.63% and −6.19% (central −5.25%). The two effects are additive because both act on the operating point and neither materially alters the epoch difference. The climate erosion term deepens accordingly to between −6.07% and −7.63%, raising the required design margin from 5.13% to between 6.1% and 7.6%.

The channels load unequally, and this is further evidence of the point made in Section 3.3. An ambient offset raises module temperature but leaves incident irradiance unchanged, and the supply pressure is irradiance-dominated; of the 3.13% per °C combined sensitivity, 2.77 points fall on demand and only 0.36 on supply. Urban heating therefore drives the divergence strongly toward demand dominance, taking the DP/SP ratio from 1.01 to above 7 at the central intensification. Along with the opposite shift produced by aging, this brackets the apparent demand–supply symmetry of Section 3.9 from both sides and confirms that it should not be treated as a general property of hot-arid NZEBs.

This result highlights a critical compounding effect: when PV degradation is considered alongside climate change, the resulting energy deficit becomes an order of magnitude larger. The DF framework can accommodate this effect directly by replacing EPV 2050 with a degradation-adjusted value, enabling combined climate-and-degradation analysis without modifications to the framework structure. This extension is essential for long-term NZEB planning and asset management.

3.14 Design and Policy Implications

The sizing calculation must distinguish between a new system designed at exact net-zero parity in 2025 and the already oversized reference array. For a new exact-parity design, the climate-erosion term indicates that an initial generation margin of approximately 5.13% relative to the 2025 electrical load would be required to maintain near-parity performance in 2050 under Scenario A. This value is specific to the adopted climate scenario and modeling assumptions and should not be interpreted as a universal PV oversizing requirement.

For the existing 51.3 kWp reference array, the 2025 surplus of 3,266 kWh absorbs most of the projected 4,044 kWh deterioration in the net energy balance between 2025 and 2050, leaving a shortfall of 778 kWh in 2050. Restoring annual parity would therefore require scaling the existing array by:

$$80{,}986/80{,}208 - 1 = 0.0097$$

This corresponds to approximately 0.97% additional PV capacity, equivalent to about 0.50 kWp or one additional 540 Wp module, subject to roof layout, module matching, and inverter-sizing constraints.

Under Scenario B, using the central literature-parameterized degradation rate of 0.8% per year, the analytically propagated PV yield in 2050 decreases to 65,616 kWh. Restoring annual parity for the existing reference array would require a capacity multiplier of:

$$80{,}986/65{,}616 = 1.234.$$

This corresponds to approximately 23.4% additional capacity relative to the existing 51.3 kWp array. For a newly sized system, the same condition is equivalent to a gross 2025 generation margin of approximately 28.5% relative to the 2025 electrical load. Because the degradation analysis is based on literature-derived rates rather than site-specific measurements, the results across the adopted degradation range of 0.5–1.0% per year should

be interpreted as sensitivity bounds rather than prescriptive design requirements.

The effects of mounting configuration and urban heat-island intensification should not be added directly to these capacity percentages as independent allowances because they interact through module operating temperature and building cooling demand. Paired EnergyPlus and PVSyst simulations using site-specific mounting, microclimate, and degradation parameters would therefore be required to establish a code-ready design allowance.

The accumulated seasonal energy deficit of approximately 8,657 kWh corresponds to roughly 9,619 kWh of energy throughput when a round-trip storage efficiency of 90% is assumed. As explained in Section 3.8, this value represents a lower bound on seasonal grid compensation rather than a battery capacity specification. Monthly aggregation does not resolve hourly charging and discharging, state-of-charge constraints, peak power requirements, or consecutive deficit periods. Consequently, this study does not provide a storage-sizing recommendation without the hourly supply–demand integration described in Section 3.8. Nevertheless, the result emphasizes the potential importance of grid-based compensation strategies, including time-of-use net metering, demand response, and distributed energy sharing.

The projected 10.02% increase in cooling electricity demand indicates that HVAC capacity and part-load performance should be reassessed using future-weather design conditions. However, the present study does not resolve future temperature extremes or undertake a dedicated equipment-sizing analysis. It therefore does not support prescribing a universal HVAC capacity allowance.

Finally, the results demonstrate that annual energy-balance metrics alone may not adequately represent the operational performance of NZEBs in hot-arid climates. The modeled seasonal DF ranges from +29.93% in winter to −29.60% in summer, while the number of grid-dependent months increases from four in 2025 to five in 2050. Although season-specific uncertainty bounds were not calculated, this pronounced modelled seasonal polarization shows how an apparently balanced annual outcome can conceal substantial intra-annual grid dependence. Reporting monthly or seasonal DF values alongside the annual energy balance could therefore provide a more informative assessment of climate resilience and grid interaction.

3.15 Application of the DF within certification frameworks

ISO 52000-1 provides an overarching framework for assessing building energy performance, in which energy balances may be calculated over monthly intervals before annual aggregation. The proposed DF could therefore be reported for each calculation interval using quantities already generated during the energy assessment. The DF is not an officially recognized ISO indicator; rather, it is proposed in this study as a voluntary supplementary disclosure alongside the weighted annual energy balance. One practical indicator would be the number of calculation intervals exhibiting a negative energy balance. For the reference building, the number of grid-dependent months increases from four in 2025 to five in 2050, revealing an aspect of grid interaction that is not apparent from the annual balance alone.

The LEED Optimize Energy Performance credit evaluates improvements in energy performance and emissions relative to an ASHRAE 90.1 Appendix G baseline using its established methodology. The DF is not a recognized LEED credit or compliance indicator. Nevertheless, as an author-proposed supplementary durability measure, it could help assess whether performance margins established under present-day weather are likely to persist over the intended assessment horizon. Renewable energy production could, for example, be evaluated using a climate-adjusted yield or reported alongside the corresponding supply pressure. For the reference system, the projected supply pressure is 2.55% in 2050 under Scenario A. Under Scenario B, the propagated 2050 yield of 65,616 kWh represents a reduction of approximately 20.2% relative to the 2025 yield of 82,220 kWh. These values should be interpreted as scenario-specific results rather than as formal ISO or LEED adjustment factors.

A further recommendation concerns the thermal modelling of rooftop PV systems. The results presented in Section 3.4 indicate that using the default thermal-loss coefficient can overestimate the delivered generation margin of

a flush-mounted rooftop array by approximately three percentage points. For the reference building, the estimated 2025 generation margin decreases from 4.14% under the simulated default coefficient to approximately 1.33% under the indicative flush-mounted condition. Declaring the assumed thermal-loss coefficient and demonstrating its consistency with the installation configuration are therefore recommended as good modelling practice when renewable energy performance is reported within either framework. This is an author recommendation and does not represent an existing ISO or LEED requirement.

Finally, the reference building retains a small gas-fired heating load of approximately 44 kWh per year. Although this quantity is negligible relative to the annual electrical balance, excluding on-site fossil-fuel consumption is inconsistent with comprehensive site-energy decarbonization. Electrifying this residual heating load would require approximately 15 kWh of additional electricity under the adopted conversion assumption, eliminate direct on-site combustion, and allow the site-energy and electrical divergence assessments to be evaluated on a consistent basis.

4. Limitations

Several limitations of this study should be acknowledged to contextualize the results and guide future research.

First, the climate projections are based on a single Global Climate Model (HadCM3) and a single emission scenario (SRES A2). The A2 warming increment of +0.93 °C for coastal Karachi falls within the CMIP6 multi-model range, and the sensitivity analysis of Section 3.11 explores the DF response to larger warming increments through the analytical transfer function of Section 2.9. However, these propagated cases are sensitivity bounds on ΔT and ΔG, not independently simulated climate scenarios: they do not capture CMIP6-specific changes in humidity, cloud structure, extreme-event frequency, or temporal variability. A multi-model ensemble analysis using CMIP6 or CORDEX-SA downscaled datasets, with morphed SSP2-4.5 and SSP5-8.5 weather files, would provide a more comprehensive quantification of uncertainty and enable probabilistic DF estimates. This is identified as the highest-priority extension.

Second, the PV degradation analysis is based on literature-derived degradation rates rather than site-specific measurements. Actual degradation in Karachi may differ due to local environmental factors such as high humidity, salt exposure from the coastal environment, elevated dust deposition, and intense ultraviolet radiation. These factors could accelerate degradation beyond global averages, implying that the long-term supply pressure (SP) may be underestimated. Future work should incorporate field-monitored degradation data to refine long-term DF projections.

Third, the simulated epochs use a thermal loss coefficient of Uc = 20.0 W/m²K, the PVSyst default (a rooftop/semi-integrated reference) that is higher than a coefficient fitted to the specific rooftop-flush installation modelled on the demand side. The consequences are quantified analytically in Section 3.4 across the range 15–20 W/m²K and are substantial for the as-built divergence, which deepens to between −2.19% and −4.59%, while leaving the climate erosion term within 0.15 percentage points. The analytical treatment is a first-order propagation calibrated against the simulated pair and validated to within one kilowatt-hour at the simulated coefficient; it is nevertheless not a substitute for a rooftop-parameterized simulation campaign, which would additionally capture the redistribution of the temperature loss across the year and any consequent change in the monthly DF profile. Such a campaign is identified as the highest-priority extension of this work.

Fourth, urban heating is treated analytically in Section 3.13 as an ambient offset propagated through the demand and thermal-supply channels, rather than through an urban canopy model coupled to the building simulation. The magnitude and the intensification rate adopted are drawn from the literature for comparable coastal arid cities and are not specific to the modelled urban block. Two consequences follow. The offset is applied as a daily-mean value, so the strong nocturnal weighting characteristic of canopy-layer urban heating in coastal cities is not resolved, and the split of the demand response between daytime cooling and overnight thermal mass charging is therefore not captured. And the analysis carries no information about the interaction between urban heating and the upper tail of the temperature distribution, which Section 2.1 identifies as already understated by the

morphing procedure. A microclimate-resolved treatment would sharpen both the magnitude and the diurnal structure of the result reported here.

Finally, the analysis is based on a single DOE reference building typology. While this approach ensures standardization and comparability, it limits the generalizability of the results across the broader building stock. Different building types such as residential, retail, and industrial facilities exhibit distinct load profiles, occupancy patterns, and HVAC characteristics, which may alter the relative contributions of demand and supply pressures. Extending the DF framework to multiple building typologies is therefore necessary to establish its applicability at the urban or national scale.

Despite these limitations, the core findings of this study particularly the dual-pressure mechanism, the strong seasonal polarization of DF, and the inadequacy of annual energy balance as a sole performance metric are expected to remain robust, as they arise from fundamental physical relationships between temperature, cooling demand, and PV efficiency.

5. Conclusion

This study introduces and applies the Net-Zero Divergence Factor (DF), a normalized and additive scalar metric designed to quantify the compound erosion of NZEB performance under climate change. Applied to a DOE reference small office building in Karachi, Pakistan, under the HadCM3 A2 scenario for the period 2025–2050, the DF captures both demand-side and supply-side climate pressures within a single, comparable indicator.

The principal result is that, within the HadCM3-A2 simulation framework, mid-century climate drift erodes 5.13% of the baseline annual load, comprising a 10.02% increase in cooling electricity (demand pressure = +2.58%) and a 2.45% reduction in PV generation (supply pressure = +2.55%). The magnitude is approximately 3.4 times the estimated deterministic annual sensitivity range of ±1.50%, but this comparison is not a formal significance test. The result is conditional on the adopted climate model, morphing procedure, and physics-based models.

For the reference rooftop system, the as-built divergence is design- and installation-dependent. At the default coefficient used in the simulations (Uc = 20 W/m²K, a rooftop/semi-integrated reference), the annual balance moves from +3,266 kWh in 2025 to −778 kWh in 2050, an as-built DF of −0.99% ± 1.50%, retained only as the simulated reference; at an indicative flush-mounted coefficient (Uc = 16 W/m²K), the divergence deepens to −3.69%. No claim of a resolved surplus-to-deficit crossing is made for any individual system. The as-built value is, moreover, conditional in a way the climate erosion term is not: propagating the thermal loss coefficient to the rooftop-flush range deepens it to between −2.19% and −4.59%, and a plausible urban heating intensification of +0.3 to +0.8 °C deepens it to between −1.93% and −3.49%. The divergence of a real rooftop array in a densifying city is therefore likely to be several times that of the nominal case, while the underlying climate signal remains the same.

The modelled seasonal divergence spans nearly sixty percentage points, from +29.93% in winter to −29.60% in summer, and the grid-dependent period expands from four to five months. These seasonal values are substantially larger than the annual sensitivity range, but no season-specific confidence bounds are claimed because seasonal uncertainty was not propagated separately. Demand and supply pressures are of comparable order in the reference simulation, although their numerical near-equality is coincidental and highly scenario-dependent.

When module degradation is incorporated using a temperature-coupled rate, the deficit deepens by an order of magnitude, to between −12.95% and −23.56% across a coastal degradation band of 0.5–1.0% per year, and the divergence becomes strongly supply-dominated. Evaluated as sensitivity bounds at warming increments of +1.3 to +1.5 °C (analytically propagated, not independently simulated SSP scenarios), the transfer function gives an annual DF between −2.14% and −4.13%, depending on the treatment of the irradiance signal, with summer deficits approaching −35% to −38%. Results in this paragraph, and all parameter excursions beyond the two simulated epochs, are obtained analytically through the propagation model of Section 2.9, which is validated against the simulated case to within one kilowatt-hour and is labeled as propagated wherever it is applied. Replacing these propagations with dedicated simulation campaigns, in particular a rooftop-

parameterized PVSyst run and a site-monitored degradation rate, is the principal outstanding requirement identified by this study.

These findings expose a structural limitation in current NZEB certification frameworks, including ISO 52000-1 and the EPBD, which define net-zero performance solely on an annual basis. In hot-arid climates, annual energy balance conceals substantial seasonal grid dependence, with direct implications for peak demand, storage requirements, and carbon accounting. Accordingly, this study supports three key recommendations: incorporation of seasonal DF profiles as a supplementary performance indicator; revision of PV sizing and storage guidelines to include climate change and degradation margins; and extension of DF-based assessments across multiple emission scenarios and building typologies in thermally similar regions.

Future research should extend the DF framework by generating CMIP6-based morphed weather files (e.g., using CORDEX-SA or ISIMIP3b downscaled SSP2-4.5 and SSP5-8.5 projections) to replace the analytical sensitivity bounds reported here with fully simulated scenario comparisons that capture humidity, cloud-structure, and temporal variability changes. Site-specific PV degradation measurements under local environmental conditions should also be incorporated. In parallel, the DF framework should be extended across building typologies and climatic zones to develop design-margin guidance for national building codes.

Overall, the results demonstrate that maintaining long-term NZEB performance requires a shift from static annual targets toward dynamic, climate-resilient design strategies. In thermally stressed regions, resilience margins rather than nominal annual net-zero parity should define the benchmark for future building energy policy.

References

[1] UNEP and Global ABC, 2024 Global Status Report for Buildings and Construction, United Nations Environment Programme, Nairobi, 2024. https://www.unep.org/resources/report/global-status-report-buildings-and-construction-20242025

[2] IEA, "Buildings — Energy System," International Energy Agency, Paris, 2023. https://www.iea.org/energy-system/buildings

[3] C. Maduta, D. D'Agostino, S. Tsemekidi-Tzeinaraki, and L. Castellazzi, "From Nearly Zero-Energy Buildings (NZEBs) to Zero-Emission Buildings (ZEBs): Current status and future perspectives," Energy and Buildings, vol. 328, pp. 115133, 2025. https://doi.org/10.1016/j.enbuild.2024.115133

[4] G. Ramos Ruiz and A. Olloqui del Olmo, "Climate Change Performance of nZEB Buildings," Buildings vol. 12 no 10 pp 1755, 2022 https://doi.org/10.3390/buildings12101755

[5] European Commission, "Energy Performance of Buildings Directive (EU) 2024/1275," Official Journal of the European Union, 8 May 2024. https://energy.ec.europa.eu/topics/energy-efficiency/energy-performance-buildings/energy-performance-buildings-directive_en

[6] S. Chaturvedi and D. Elangovan, "Identification of climate adaptive multivariate optimization methodologies for the design of NZEB in India: a holistic review," Frontiers in Energy Efficiency, vol. 2, pp. 1430647, 2024. https://doi.org/10.3389/fenef.2024.1430647

[7] F. Ascione, R. F. De Masi, A. Gigante, and G. P. Vanoli, "Resilience to the climate change of nearly zero energy-building designed according to the EPBD Recast," Energy and Buildings, vol. 256, pp. 111739, 2022. https://doi.org/10.1016/j.enbuild.2022.112004

[8] X. Chen, H. Mao, N. Cheng, L. Ma, Z. Tian, Y. Luo, C. Zhou, H. Li, Q. Wang, W. Kong, and J. Fan, "Climate change impacts on global photovoltaic variability," Applied Energy, vol. 374(C), 2024. https://doi.org/10.1016/j.apenergy.2024.124087

[9] Wu, H., Kong, Q., Huber, M., Sun, M., & Craig, M. T. (2026). Climate change will increase high-temperature risks, degradation, and costs of rooftop photovoltaics globally. Joule, 10(1), https://doi.org/10.1016/j.joule.2025.102218

[10] M. Bughio, M. S. Khan, W. A. Mahar, and T. Schuetze, "Impact of Passive Energy Efficiency Measures on Cooling Energy Demand in an Architectural Campus Building in Karachi, Pakistan," Sustainability, vol. 13, no. 13, pp. 7251, 2021. https://doi.org/10.3390/su13137251

[11] S. Summa, L. Tarabelli, G. Ulpiani, and C. Di Perna, "Impact of Climate Change on the Energy and Comfort Performance of nZEB: A Case Study in Italy," Climate, vol. 8, no. 11, pp. 125, 2020. https://doi.org/10.3390/cli8110125

[12] R. F. De Masi and others, "Impact of weather data and climate change projections in the refurbishment design of residential buildings in cooling dominated climate," Applied Energy, vol.

303, pp. 117591, 2021. https://doi.org/10.1016/j.apenergy.2021.117584

[13] IPCC, Climate Change 2021: The Physical Science Basis. Contribution of Working Group I to the Sixth Assessment Report of the IPCC, V. Masson-Delmotte and others, Eds., Cambridge University Press, 2021. https://doi.org/10.1017/9781009157896

[14] IPCC, Climate Change 2023: Synthesis Report, H. Lee and J. Romero, Eds., IPCC, Geneva, 2023. https://doi.org/10.59327/IPCC/AR6-9789291691647

[15] A. M. Khourchid, T. A. Al-Ansari, and S. G. Al-Ghamdi, "Cooling Energy and Climate Change Nexus in Arid Climate and the Role of Energy Transition," Buildings, vol. 13, no. 4, pp. 836, 2023. https://doi.org/10.3390/buildings13040836

[16] Scoccimarro, E., Cattaneo, O., Gualdi, S. et al., "Country-level energy demand for cooling has increased over the past two decades," Communications Earth & Environment, vol. 4, pp. 198, 2023. https://doi.org/10.1038/s43247-023-00878-3

[17] E. Ahmadian, C. Bingham, A. Elnokaly, B. Sodagar, and I. Verhaert, "Impact of Climate Change and Technological Innovation on the Energy Performance and Built Form of Future Cities," Energies, vol. 15, no. 22, pp. 8592, 2022. https://doi.org/10.3390/en15228592

[18] S. E. Belcher, J. N. Hacker, and D. S. Powell, "Constructing design weather data for future climates," Building Services Engineering Research and Technology, vol. 26, no. 1, pp. 49–61, 2005. https://doi.org/10.1191/0143624405bt112oa

[19] M. F. Jentsch, A. S. Bahaj, and P. A. B. James, "Climate change future proofing of buildings — Generation and assessment of building simulation weather files," Energy and Buildings, vol. 40, no. 12, pp. 2148–2168, 2008. https://doi.org/10.1016/j.enbuild.2008.06.005

[20] M. Deru, K. Field, D. Studer, K. Benne, B. Griffith, P. Torcellini, and others, U.S. Department of Energy Commercial Reference Building Models of the National Building Stock, National Renewable Energy Laboratory, NREL/TP-5500-46861, 2011. https://www.researchgate.net/publication/262107107_US_Department_of_Energy_Commercial_Reference_Building_Models_of_the_National_Building_Stock

[21] C. Gordon, C. Cooper, C. A. Senior, H. Banks, J. M. Gregory, T. C. Johns, J. F. B. Mitchell, and R. A. Wood, "The simulation of SST, sea ice extents and ocean heat transports in a version of the Hadley Centre coupled model without flux adjustments," Climate Dynamics, vol. 16, pp. 147–168, 2000. https://doi.org/10.1007/s003820050010

[22] ASHRAE, ANSI/ASHRAE/IESNA Standard 90.1-2004: Energy Standard for Buildings Except Low-Rise Residential Buildings, American Society of Heating, Refrigerating and Air-Conditioning Engineers, Atlanta, 2004.

[23] M. F. Jentsch, P. A. B. James, L. Bourikas, and A. S. Bahaj, "Transforming existing weather data for worldwide locations to enable energy and building performance simulation under future climates," Renewable Energy, vol. 55, pp. 514–524, 2013. https://doi.org/10.1016/j.renene.2012.12.049

[24] P. Gonçalves and others, "Effectiveness of CCWorldWeatherGen weather file generation tool," Ambiente Construído, 2024. https://doi.org/10.1590/s1678-86212024000100771

[25] Mohamed Imam, Yu Chen and Tyrone Marshall, "Integrating Climate Change Projections in Building Performance Simulations: Case Study of 17 North American Cities," Journal of Architectural Engineering, vol. 29, no. 3, 2023. https://doi.org/10.1061/JAEIED.AEENG-1593

[26] H. van Dijk and others, "The new EN ISO 52000 family of standards to assess the energy performance of buildings put in practice," REHVA Journal, 2019.

[27] Mashaly, A., Elmadawy, M., Elgohary, M. et al. "Novel and cost-efficient design of stand-alone PV system with simulation using PVsyst and experimental validation," Scientific Reports, vol. 15, pp. 1–17, 2025. https://doi.org/10.1038/s41598-025-28401-y

[28] S. Bentouba, M. Bourouis, N. Zioui, A. Pirashanthan, and D. Velauthapillai, "Performance assessment of a 20 MW photovoltaic power plant in a hot climate using real data and simulation tools," Energy Reports, vol. 7, pp. 8087–8099, 2021. https://doi.org/10.1016/j.egyr.2021.10.082

[29] M. W. Anwar, Z. Ali, A. Javed, and others, "Analysis of the effect of passive measures on the energy consumption and zero-energy prospects of residential buildings in Pakistan," Building Simulation, vol. 14, pp. 1325–1342, 2021. https://doi.org/10.1007/s12273-020-0729-8

[30] X. Hou, M. Wild, D. Folini, S. Kazadzis, and J. Wohland, "Climate change impacts on solar power generation and its spatial variability in Europe based on CMIP6," Earth System Dynamics, vol. 12, no. 4, pp. 1099–1113, 2021. https://doi.org/10.5194/esd-12-1099-2021

[31] D. Yadav, S. Khatoon, J. Singh, and R. B. Singh, "Experimental analysis of elevated temperature and soiling loss on rooftop PV modules performance under composite climatic conditions,"

Scientific Reports, vol. 15, pp. 16622, 2025. https://doi.org/10.1038/s41598-025-25846-z

[32] W. S. Ebhota and P. Y. Tabakov, "Influence of photovoltaic cell technologies and elevated temperature on photovoltaic system performance," Ain Shams Engineering Journal, vol. 14, no. 7, pp. 101984, 2023. https://doi.org/10.1016/j.asej.2022.101984

[33] Zakari Y, Vuille F and Lehning M, "Climate Change Impact Assessment for Future Wind and Solar Energy Installations in India," Frontiers in Energy Research, vol. 10, pp. 859321, 2022. https://doi.org/10.3389/fenrg.2022.859321

[34] Olusola Bamisile, Caroline Acen, Dongsheng Cai, "The environmental factors affecting solar photovoltaic output," Renewable and Sustainable Energy Reviews, vol. 204, pp. 114793, 2024. https://doi.org/10.1016/j.rser.2024.115073

[35] A. Mastrucci and others, "Cooling access and energy requirements for adaptation to heat stress in megacities," Mitigation and Adaptation Strategies for Global Change, vol. 27, pp. 41, 2022. https://doi.org/10.1007/s11027-022-10032-7

[36] Zhang L, Zhang Q, Rafiq MA. The economic and environmental analysis of solar energy development under climate impacts. Science Progress. 2022;105(3). https://doi.org/10.1177/00368504221124065

[37] M. Khan, M. M. Khan, M. Irfan, and others, "Energy performance enhancement of residential buildings in Pakistan by integrating phase change materials in building envelopes," Energy Reports, vol. 8, pp. 9290–9307, 2022. https://doi.org/10.1016/j.egyr.2022.07.047

[38] Ahsan Mustafa, Muhammad Anwar, & Talha Irfan Khan. (2024). Energy optimization of an institutional building to reduce the energy and air conditioning demand. Journal of Building Engineering, https://doi.org/10.1016/j.jobe.2024.111309

[39] ISO, ISO 52000-1:2017 — Energy performance of buildings — Overarching EPB assessment — Part 1: General framework and procedures, International Organization for Standardization, 2017. https://www.iso.org/standard/65601.html

[40] B. Aboagye, S. Gyamfi, E. A. Ofosu, and S. Djordjevic, "Degradation analysis of installed solar photovoltaic (PV) modules under outdoor conditions in Ghana," Energy Reports, vol. 7, pp. 6921–6932, 2021. https://doi.org/10.1016/j.egyr.2021.10.046

[41] Atia, D.M., Hassan, A.A., El-Madany, H.T. et al. Degradation and energy performance evaluation of mono-crystalline photovoltaic modules in Egypt. Sci Rep 13, 13066 (2023).https://doi.org/10.1038/s41598-023-40168-8